USGS Report to the CEOS WGCV 35

September 24 – 28, 2012

Hyderabad, India

Greg Stensaas – USGS
Gyanesh Chander – SGT/USGS

U.S. Department of the Interior

U.S. Geological Survey

USGS
science for a changing world

NASA

LANDSAT

Four Decades of Earth Observation

1972–2012

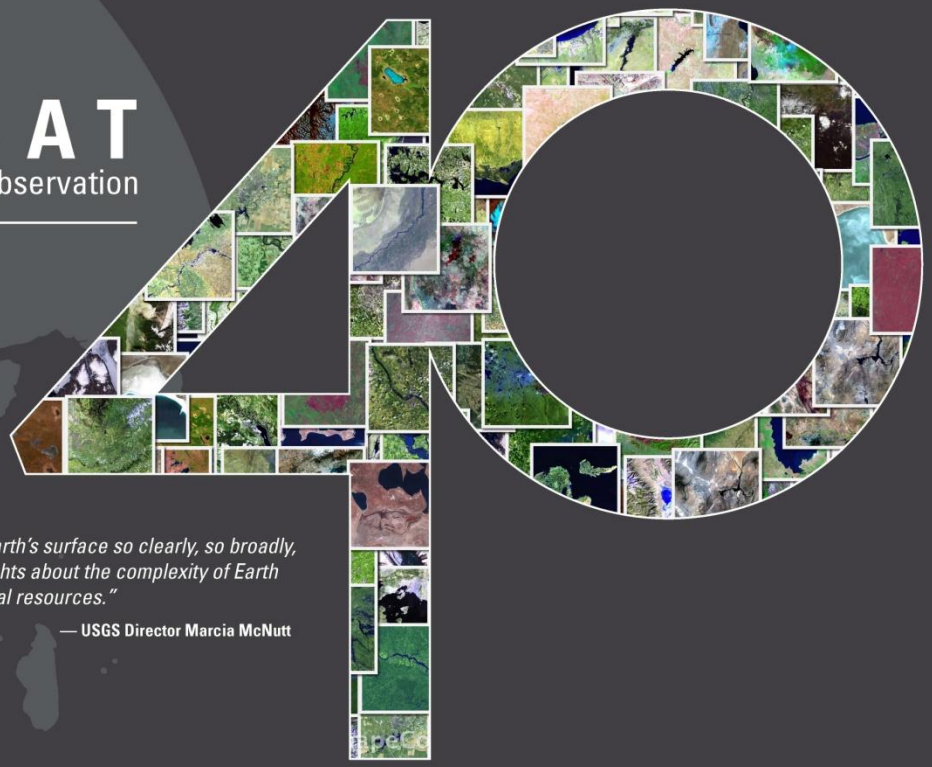

"Because Landsat enables us to see Earth's surface so clearly, so broadly, so objectively, we gain invaluable insights about the complexity of Earth systems and the condition of our natural resources."

— USGS Director Marcia McNutt

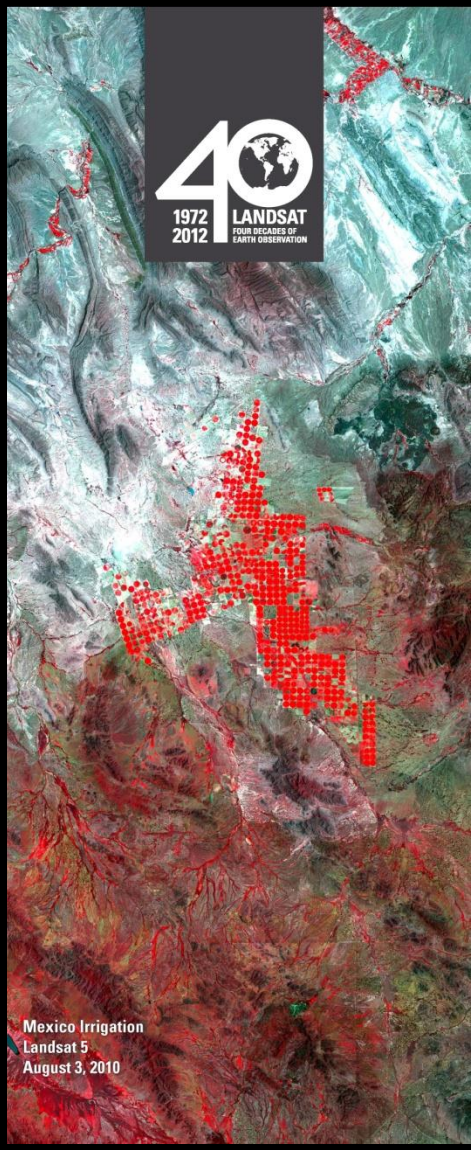

U.S. Landsat Archive (September 2012)

- **ETM+: Landsat 7**
  - 1,446,000 scenes
    - ~1,343 TB Raw and L0Ra Data
    - average scene size 487 MB
- **TM: Landsat 4 & Landsat 5**
  - 1,342,240 scenes
    - ~673 TB Raw and L0Ra Data
    - average scene size 263 MB
- **MSS: Landsat 1 through 5**
  - 610,997 scenes
    - ~37 TB Raw and L0Ra Data
    - average scene size 32 MB
- **Total:**
  - 3,399,237 scenes
    - ~2,053 TB Raw and L0Ra Data

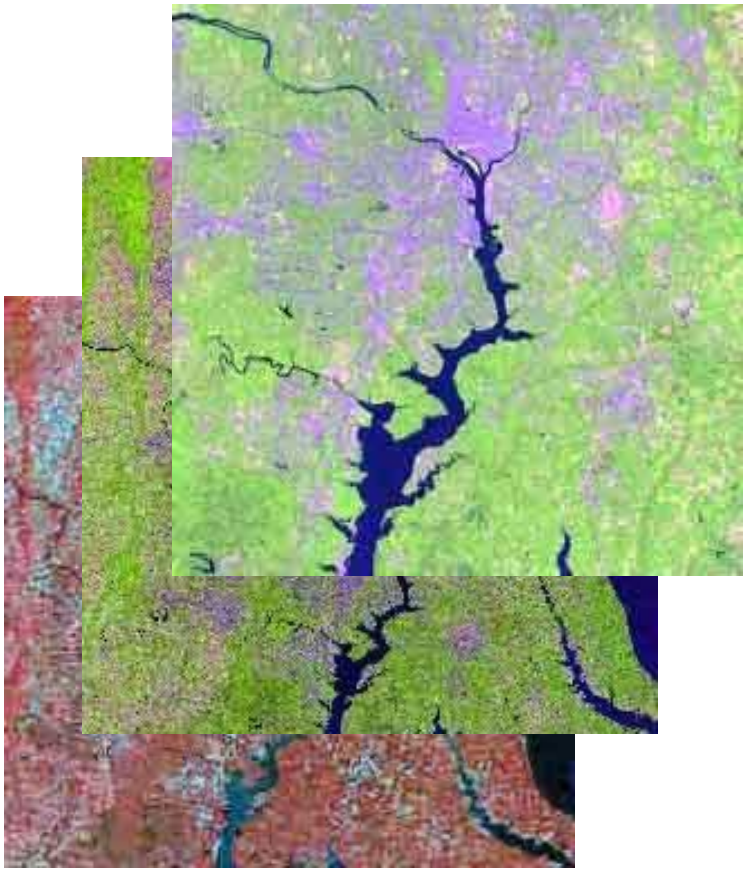

Landsat Key Accomplishments since last meeting

- **Landsat 40th Anniversary**
  - Landsat 1 Launched July 23, 1972
- **Landsat 7 – Collision avoidance maneuver (4/17/2012)**
- **Landsat 5 – Happy 28th Birthday!**
  - Downlink of MSS data
  - X-band transmitters declared failed
- **Web-enabling: distributed >9 M images since 2008**
- **Full Resolution Browse: ~60% of archive complete**
- **LandsatLook – new interface for Full Resolution Browse**
- **Landsat Metadata updated in preparation for LDCM**
- **Completed Global Land Survey 2010 (GLS2010)**

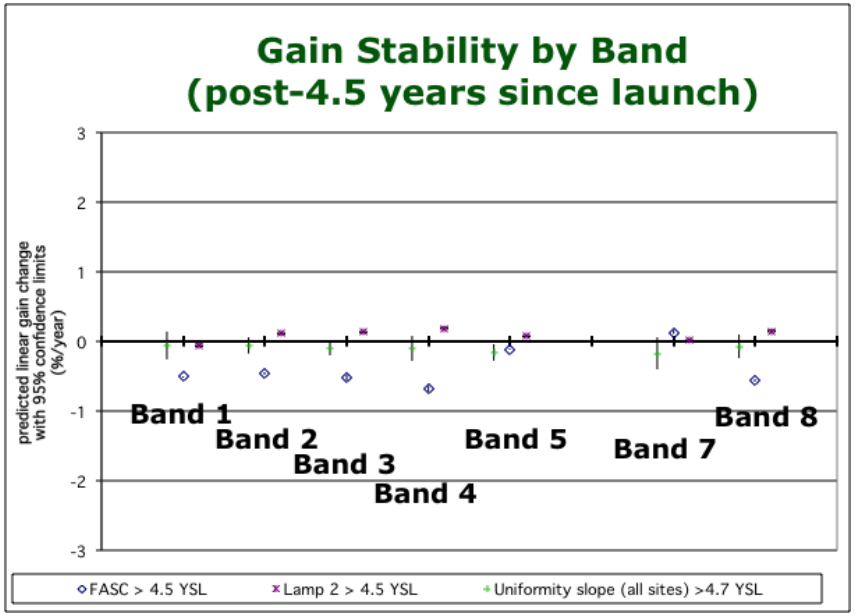

Overall variations in ETM+ gain trends are within the 5% uncertainty limit

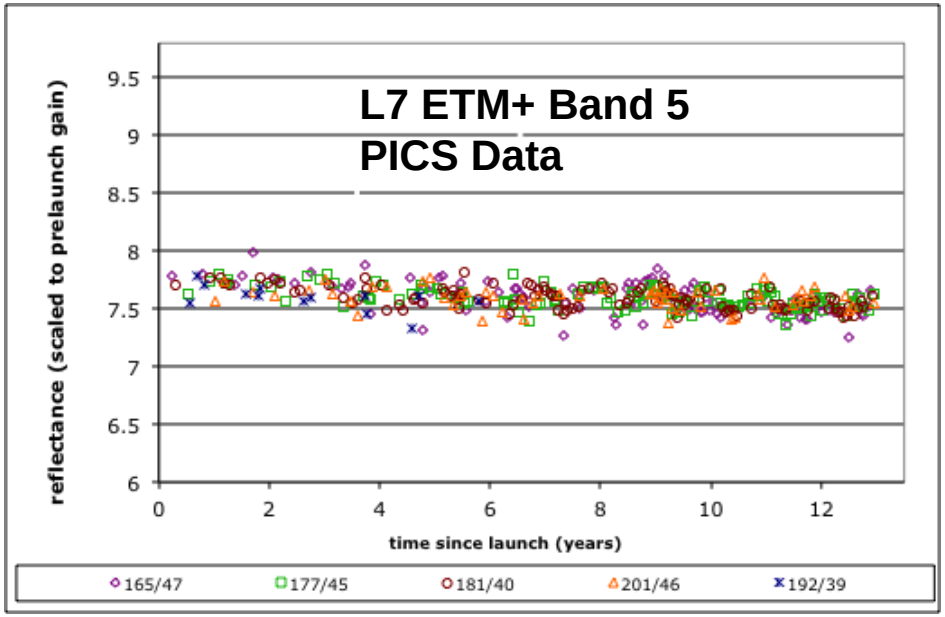

ETM+ gains estimated using PICS suggest a decay on the order of up to 0.2% per year

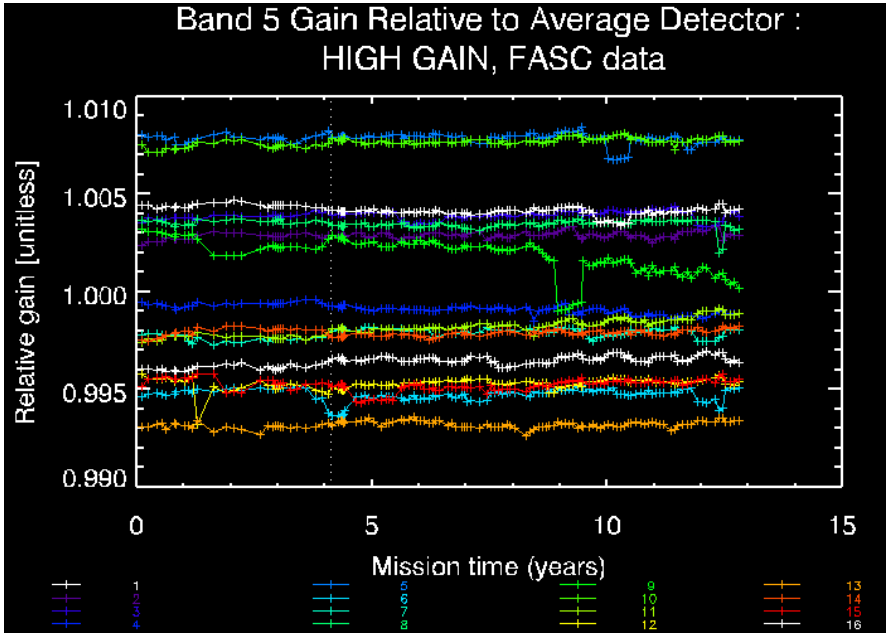

Detectors have very stable relative gains

L7 ETM+ Calibration Update

- Absolute radiometric accuracy better than ± 5% (reflective) and 1 K (thermal)
- Relative detector-to-detector normalization, i.e., striping less than ± 0.1%
- Noise stable over mission life
- SLC failure had no significant impact on L7 ETM+ reflective band radiometry- continues to be excellent

L5 TM Calibration Update

- **Within-band within-scene internal stability**
  - Scan-Correlated Shift (SCS) of up to 0.7 DN
    - Correctable with scan line-by-scan line background subtraction
  - Memory effect of up to 4 DN
    - Currently corrected in LPGS processing
- **Between-date stability**
  - Interference cycling from icing on B5 and B7
    - Correctable with IC processing or LUT that includes interference cycling
- **Radiometric calibration processing**
  - Uses Gain Calibration History stored in Look-Up Table (LUT)
  - Extracts and applies biases on a scan line by scan line basis
  - Rescaled to Fixed Radiance Range (LMIN, LMAX)
  - LUT revised April 2, 2007 to reflect revised trends from Sahara desert site data obtained from ESA
  - The L5 TM radiometric calibration uncertainty of the at-sensor spectral radiances is around 5% and is somewhat worse for early years, when the sensor was changing more rapidly, and better for later years

Cross-calibration of L5 TM & L7 ETM+

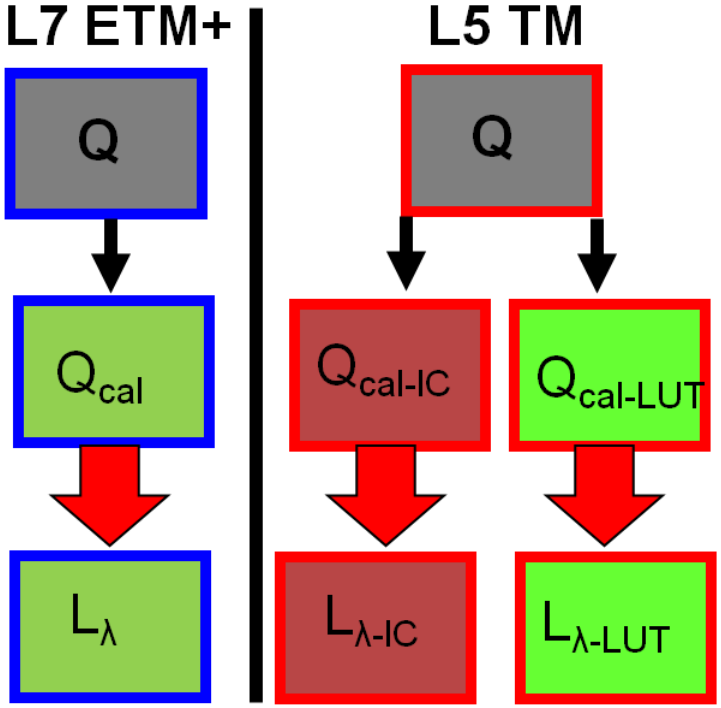

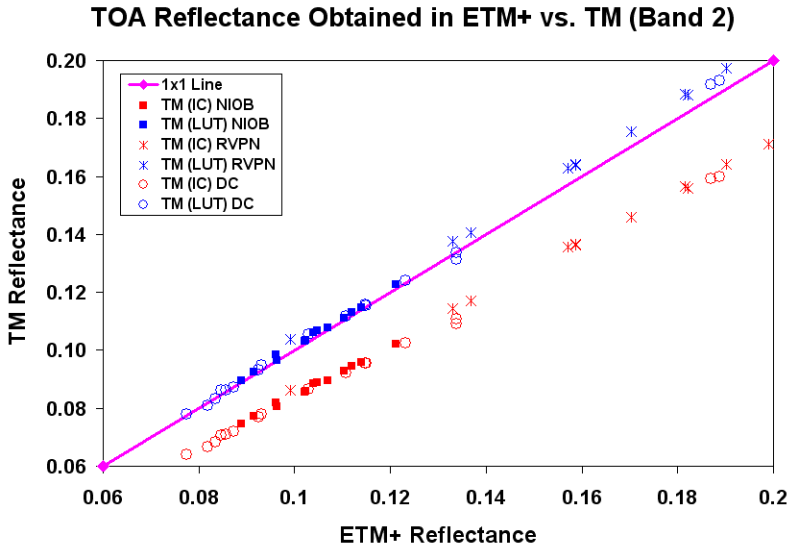

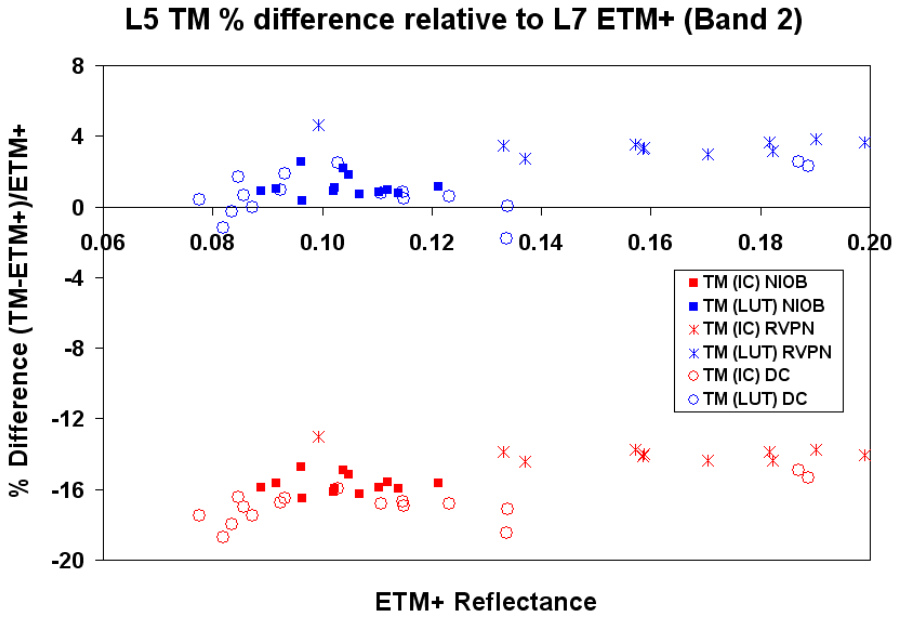

The percentage mean difference in reflectance measurements obtained from the L5 TM relative to ETM+ in **Band 2** is reduced from about **15.6% (using IC) to 1.8% (using LUT)**

USGS

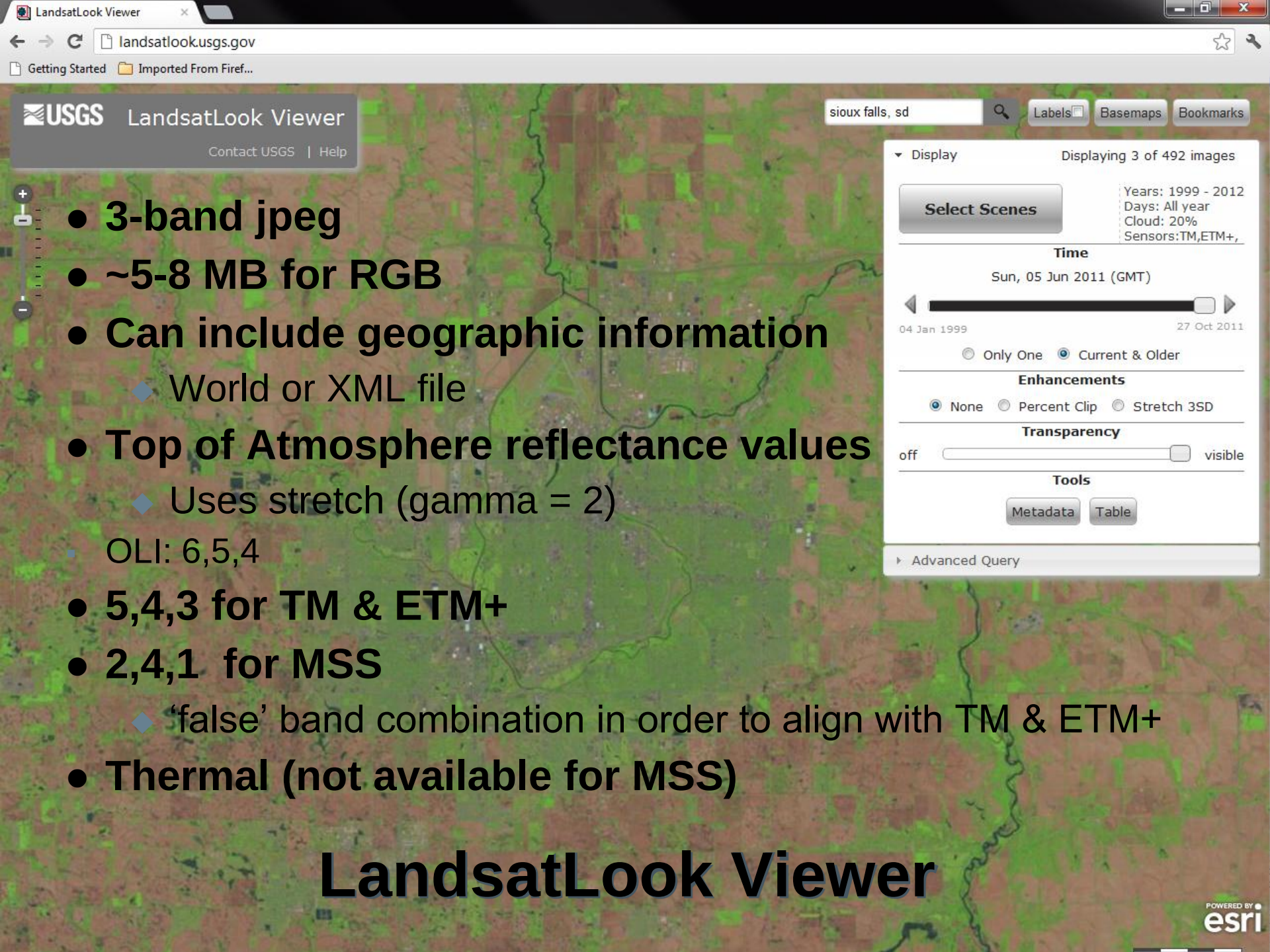

- **3-band jpeg**
- **~5-8 MB for RGB**
- **Can include geographic information**
  - World or XML file
- **Top of Atmosphere reflectance values**
  - Uses stretch (gamma = 2)
  - OLI: 6,5,4
- **5,4,3 for TM & ETM+**
- **2,4,1 for MSS**
  - 'false' band combination in order to align with TM & ETM+
- **Thermal (not available for MSS)**

LandsatLook Viewer

LGAC Progress Distribution of new global data

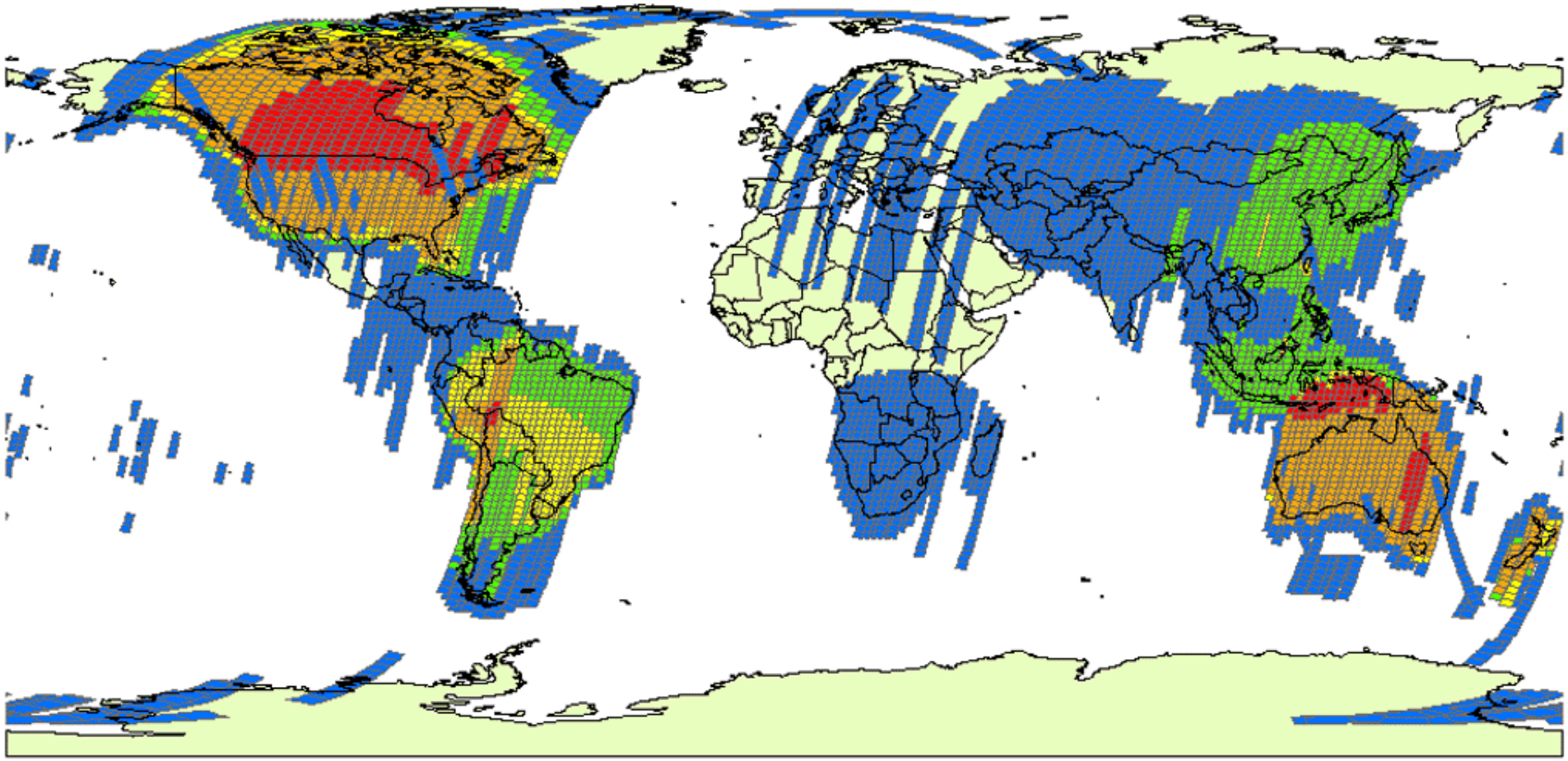

LGAC WRS2 Scenes
Status as of July 31, 2012
Acquisition Date Range: August 22, 1982 through July 30, 2012
1,051,226 Total Scenes Acquired
8,580 Unique Path/Rows

1 - 61 | 62 - 155 | 156 - 258 | 259 - 369 | 370 - 526

http://landsat.usgs.gov/about/

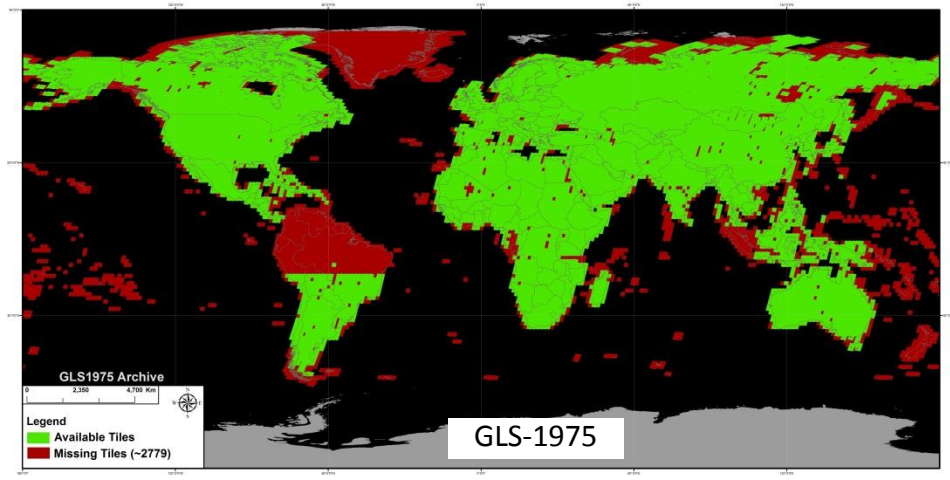

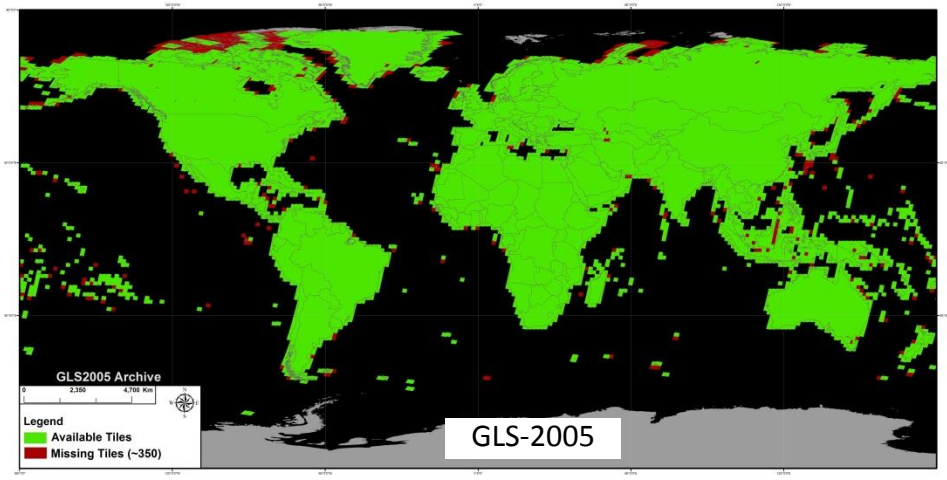

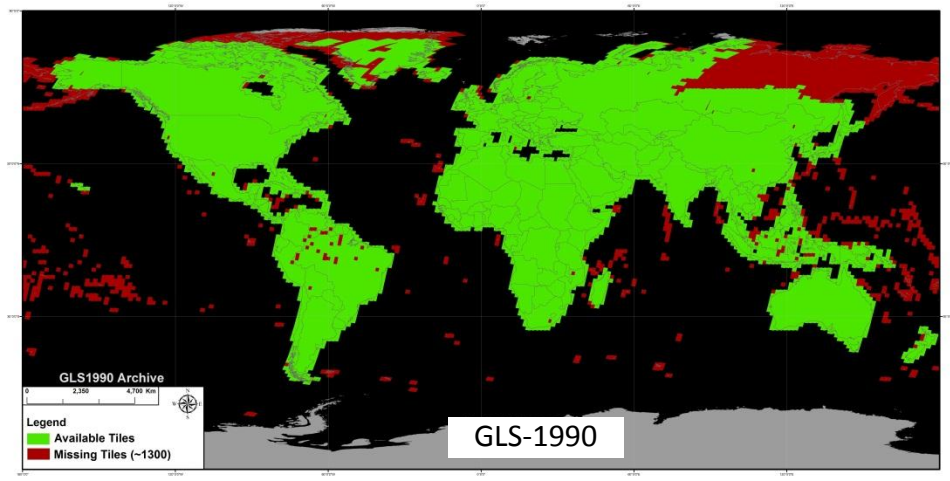

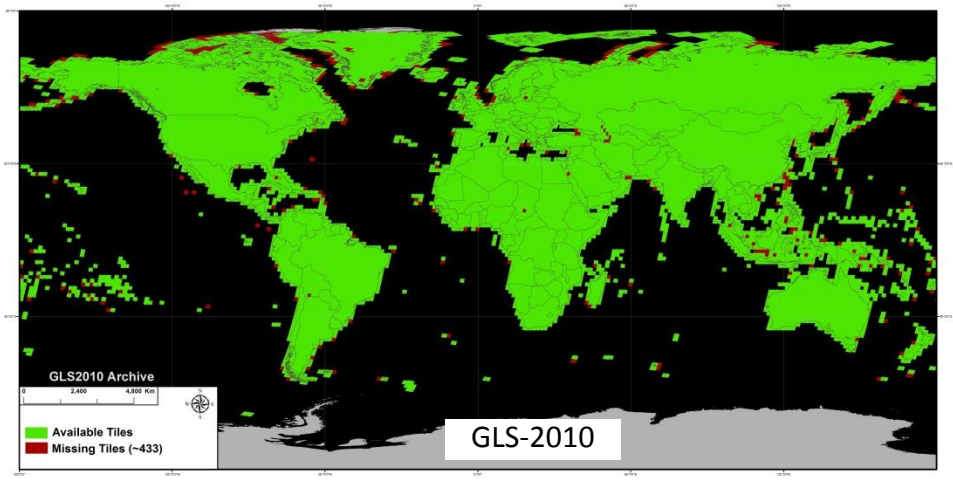

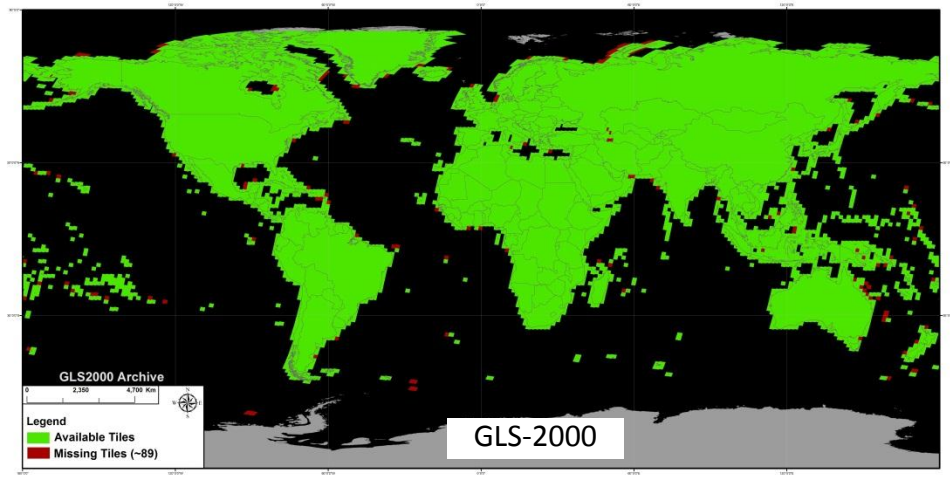

Global Land Survey (GLS)

Spatial coverage of the five GLS data sets.

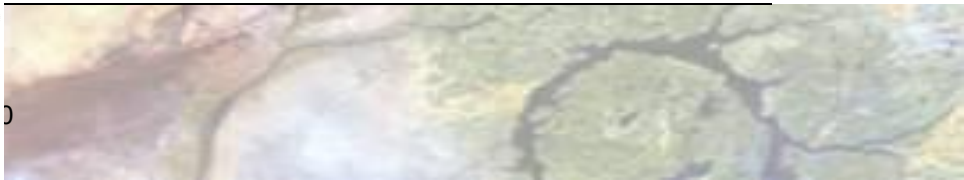

Yearly distribution of the GLS datasets. The fat bars indicate number of Landsat tiles. The percentage of those tiles in each GLS dataset is shown by the slim bars.

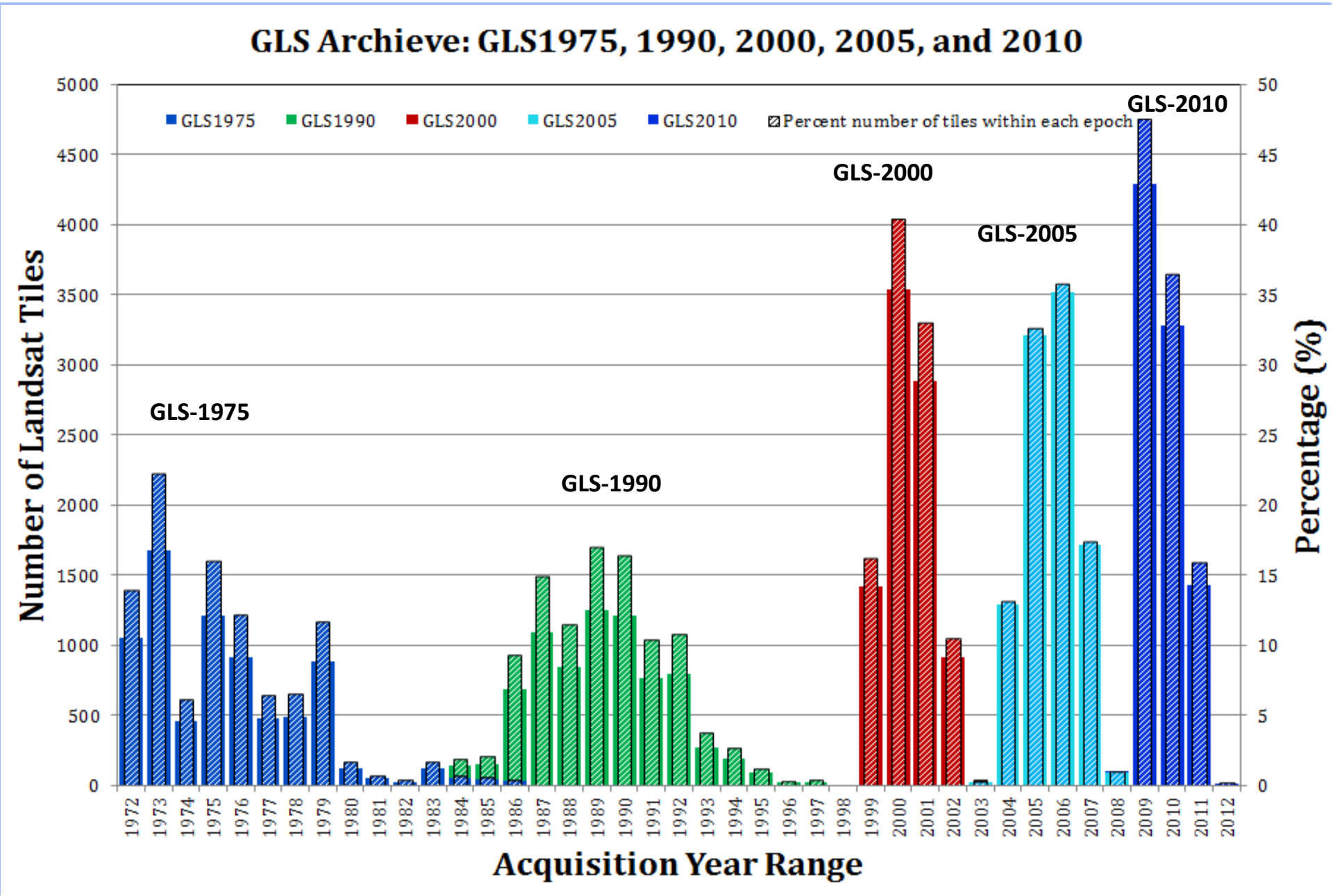

Geolocation errors (RMSE) relative to GLS 2000 in GLS 1975, GLS 1990, GLS 2005, and GLS 2010.

Dataset	Number of Images Analyzed	RMSE (m)		
		North-south	East-west	Overall
GLS 1975	6139	18.2	17.0	24.9
GLS 1990	6511	7.8	8.1	11.2
GLS 2005	7888	4.7	5.1	5.9
GLS 2010	7362	4.3	4.0	5.1

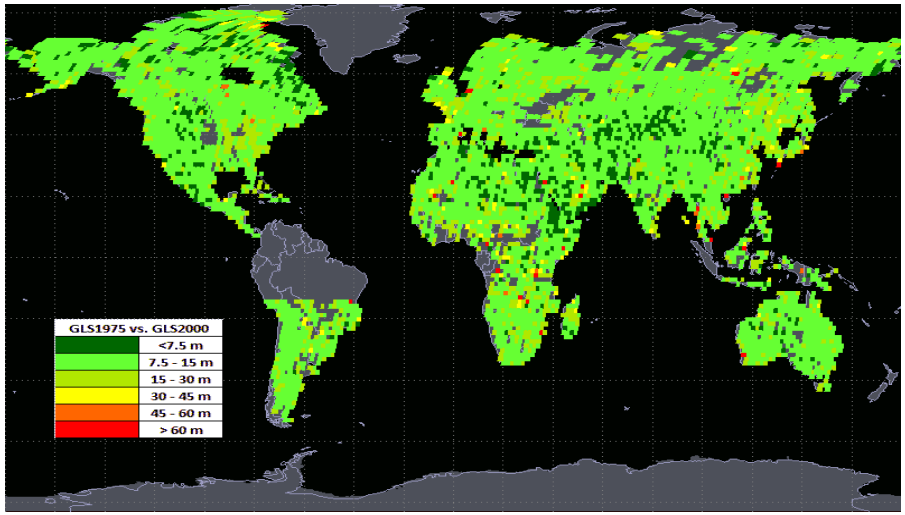

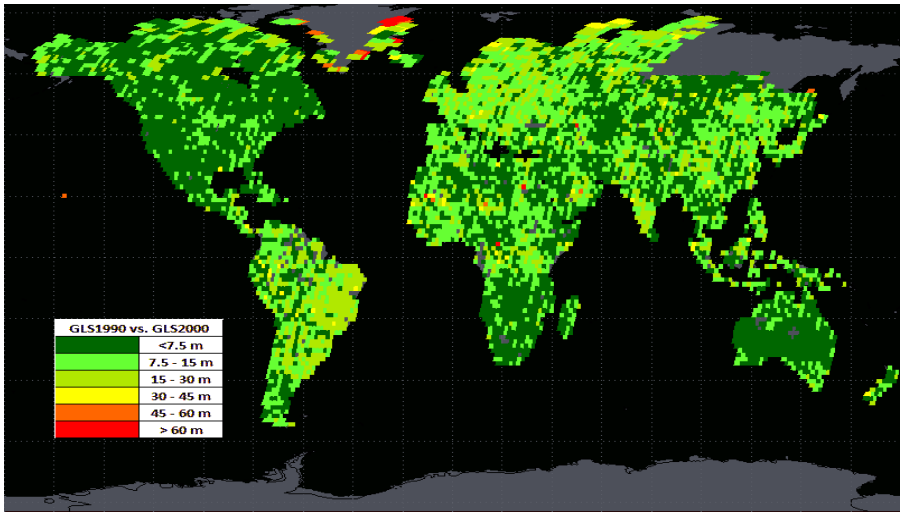

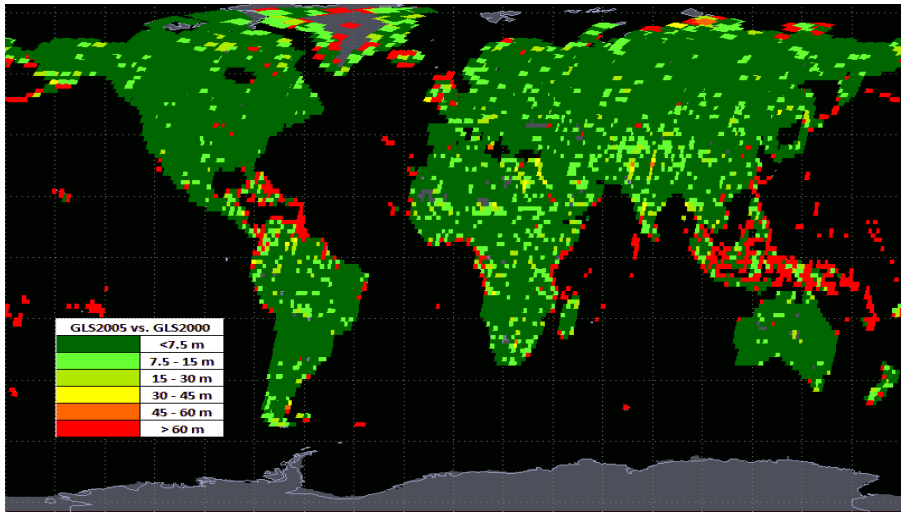

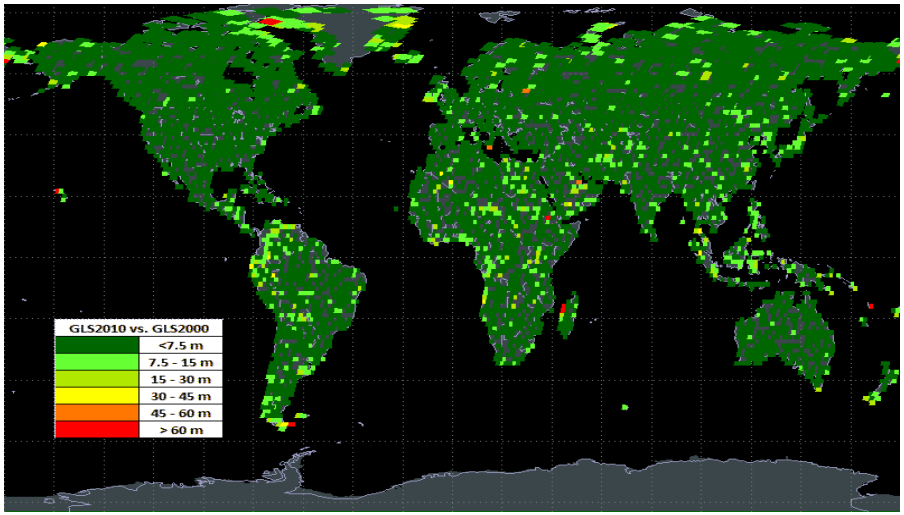

L5 TM Spatial Distribution of the Band 3 Rescaling Gains

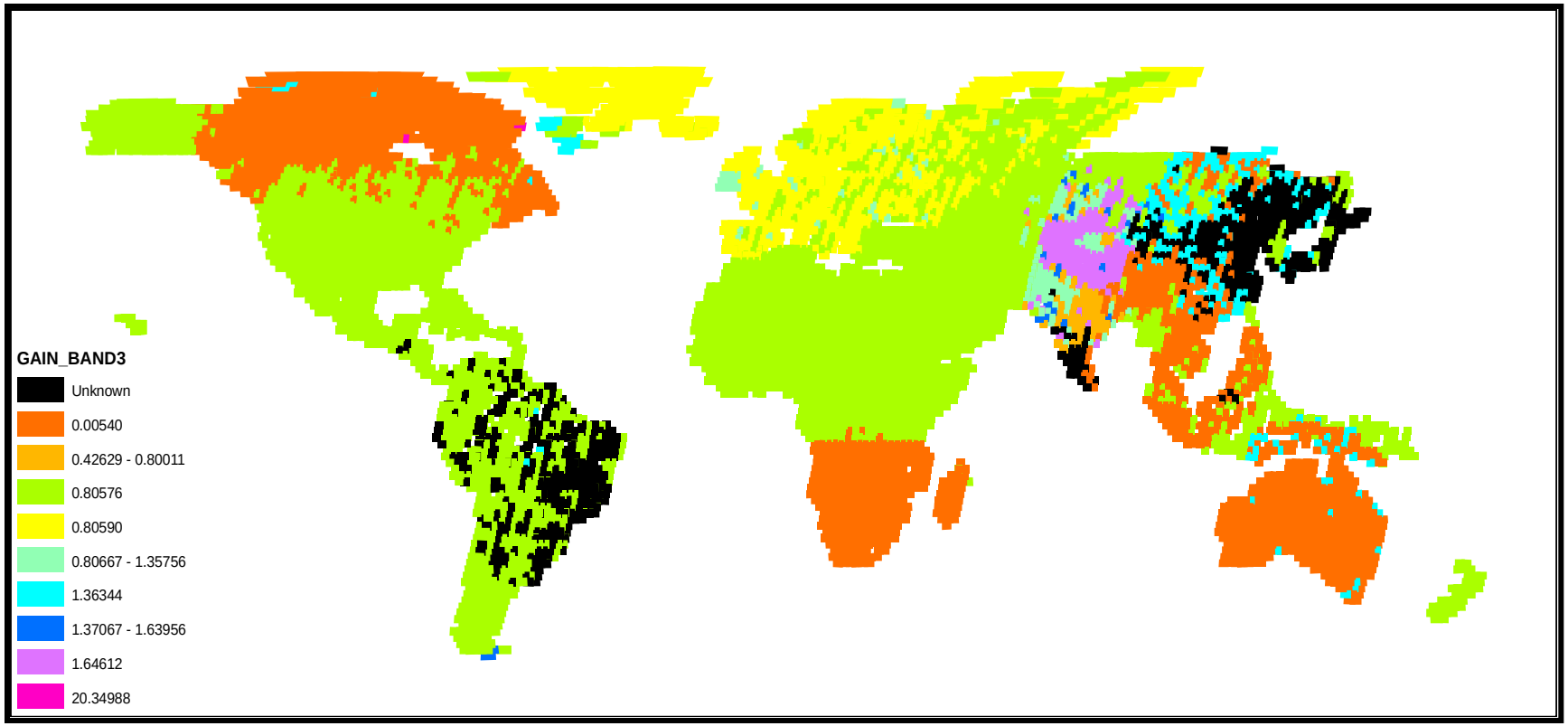

Spatial distribution of the Band 3 rescaling gains provided in the metadata of GLS 1990 images. Other bands have the same spatial patterns though the values are different. The USGS archived TM scenes are processed using a consistent radiometric calibration procedure (IC-based); however, the IGS data were processed using multiple calibration approaches resulting in different gain coefficients, and some of these images have missing header information. Calculation of accurate biophysical and geophysical variables using the GLS1990 images is not possible because the rescaling coefficients are inconsistent and sometimes not documented in the metadata file

Candidate Landsat ECVs

Terrestrial ECV	Technical Consideration			Requirements / Demand		
	Landsat Potential	USGS Readiness	USGS Uniqueness	USGS Relevance	Importance to DOI	Overall Community Demand
*Land Cover	High	High	High	High	High	High
*Leaf Area Index	High	Low	Low	Medium	Medium	Medium
FPAR	High	Low	Low	Medium	Low	Low
Biomass	Low	Low	Low	High	High	High
*Albedo	Medium	Low	Low	Medium	Low	Low
*Fire Disturbance	Medium	High	Medium	High	High	High
*Surface Water	High	High	Medium	High	High	Medium
*Snow / Ice	Medium	Medium	Low	Medium	Medium	Medium
Soil Moisture	Low	Medium	Low	Medium	Medium	Medium

*ECVs with highest initial potential for development

Prescriptive Levels of Processing

Provide users with the product most suitable to their needs

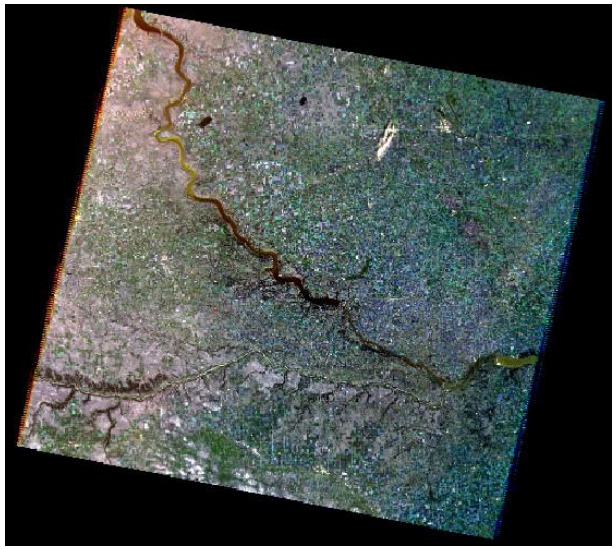

Scaled DNs

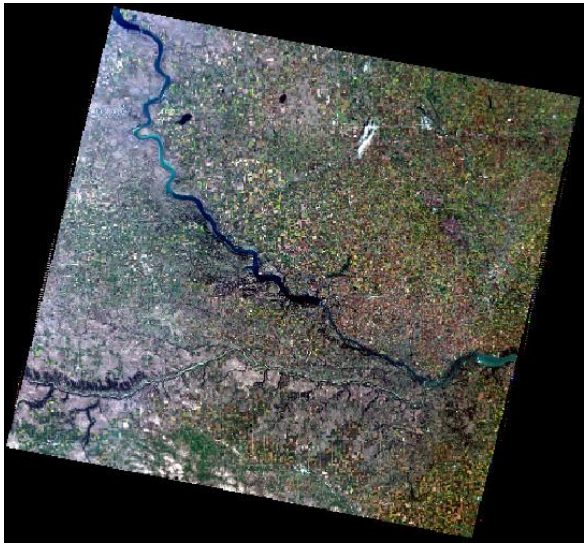

TOA Reflectance

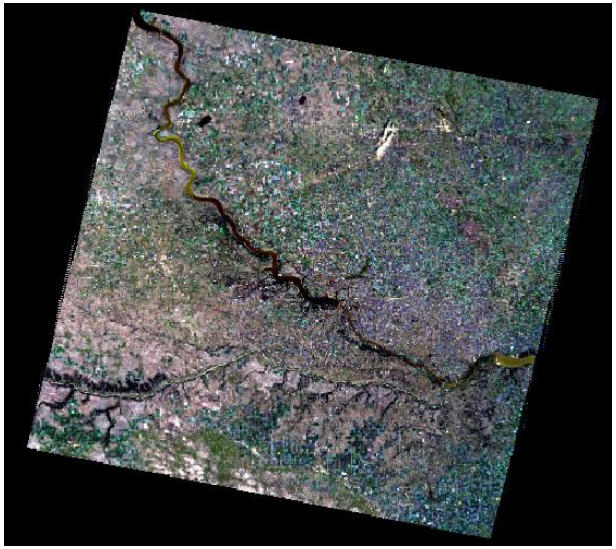

Surface Reflectance

Surface Reflectance

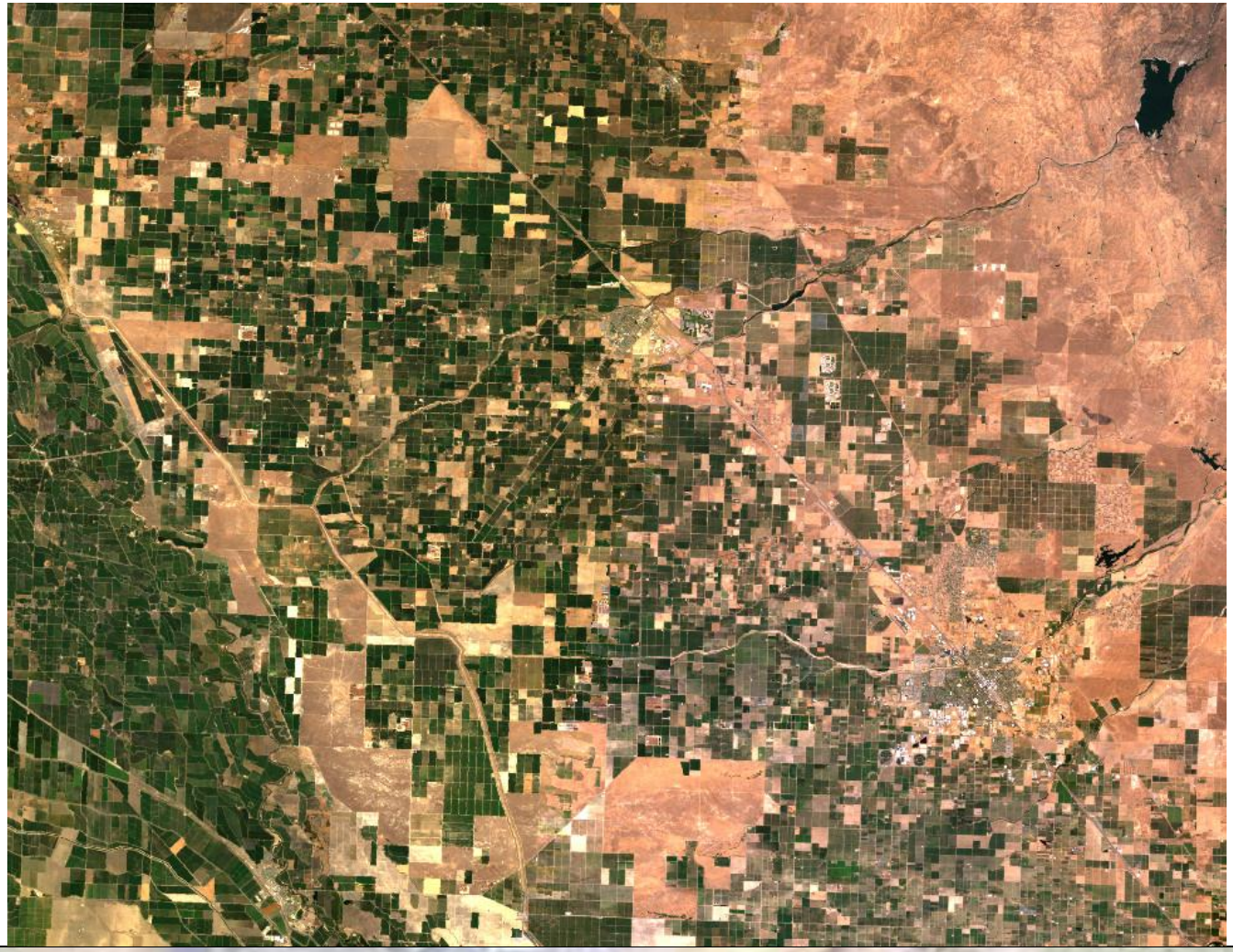

43/34
07/22/2007

42/34
07/28/2006

Moving from Data to Information

L1T At-sensor Radiance (FCDR)

Surface Reflectance (TCDR)

Leaf Area Index (ECV)

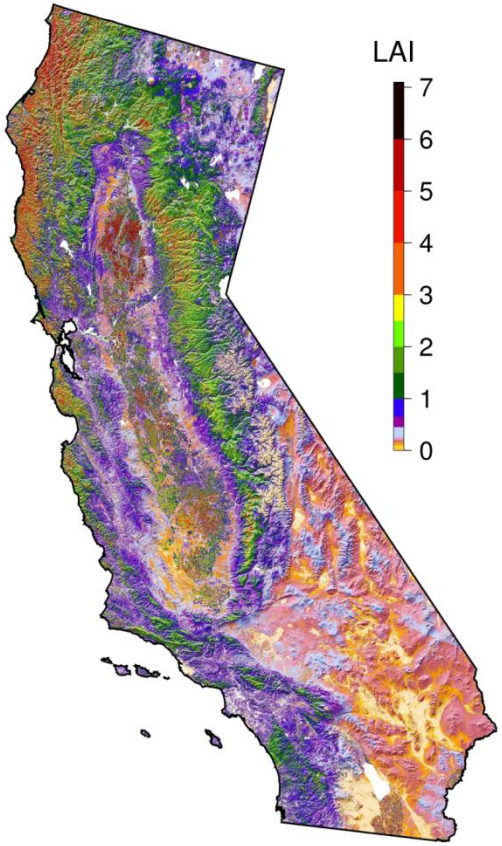

USGS

(Nemani, NASA)

Landsat Data Continuity Mission (LDCM)

The Landsat Data Continuity Mission (LDCM) is under development for a February 2013 launch. Developed as a NASA / USGS partnership

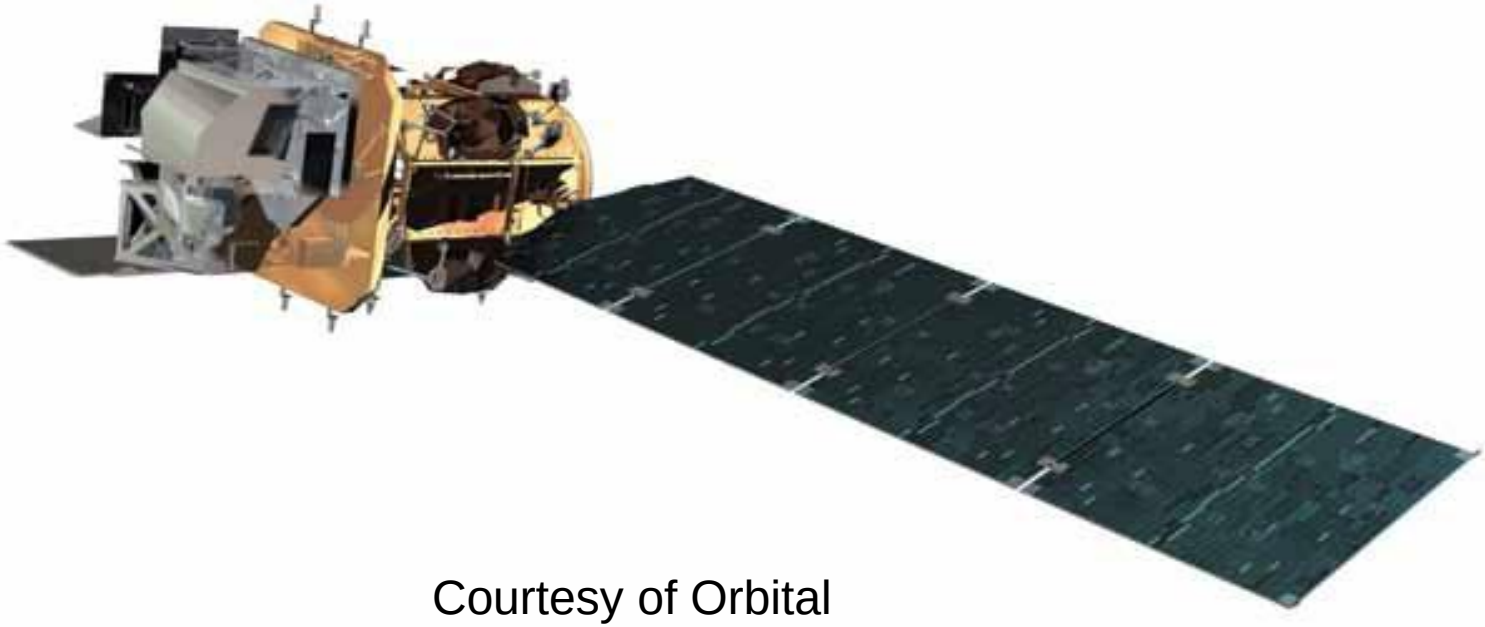

Courtesy of Orbital

NASA /USGS Mission Responsibilities

Space Segment

Operational Land Imager
- Multi-Spectral Imaging Instrument
- Pushbroom VIS/SWIR sensor
- Four mirror telescope
- FPA consisting of 14 SCAs

Thermal Infrared Sensor
- 2 thermal channels
- Pushbroom design
- QWIP detectors
- Actively cooled FPA

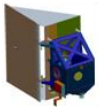

Spacecraft
- 3-axis stabilized
- Accommodated OLI & TIRS

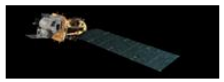

Launch Segment

Atlas V 401

Ground System

Ground Network Element (GNE)
Antenna & associated equipment for X-Band image & S-Band telemetry data downlink reception and generation of S-Band command uplink

Collection Activity Planning Element (CAPE)
Generates high level imaging mission schedules

Mission Operations Element (MOE)
Mission planning & scheduling, command & control, monitoring and analysis, flight dynamics & onboard memory management

Data Processing and Archive System (DPAS)
- Ingests and generates L0Ra data from GNE-provided Mission data
- Stores and archives LDCM data (Mission, L0Ra, and product)
- Provides inventory and metrics database services
- Provides Product Generation, Image Assessment, & Subsetter
- Provides web interface to facilitate: data discovery, product selection & ordering (for Cal/Val), & product distribution

Blue – NASA
Green - USGS

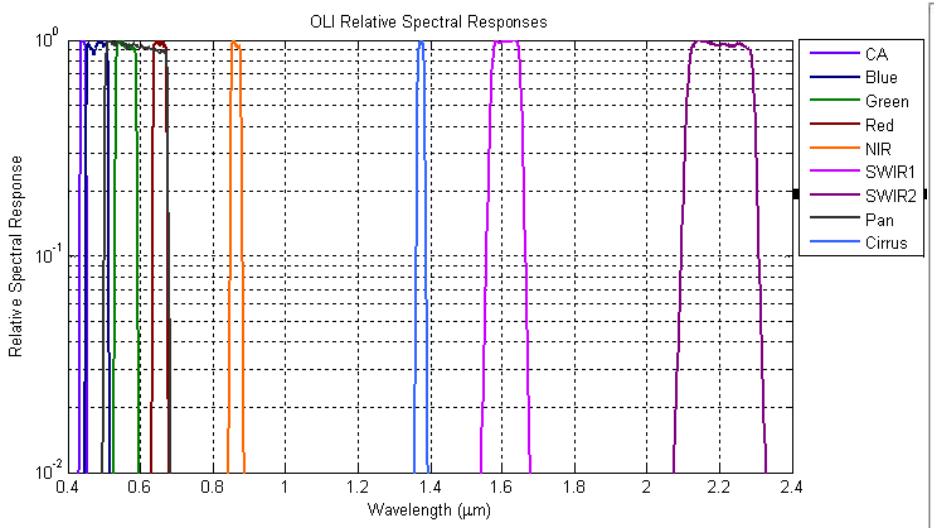

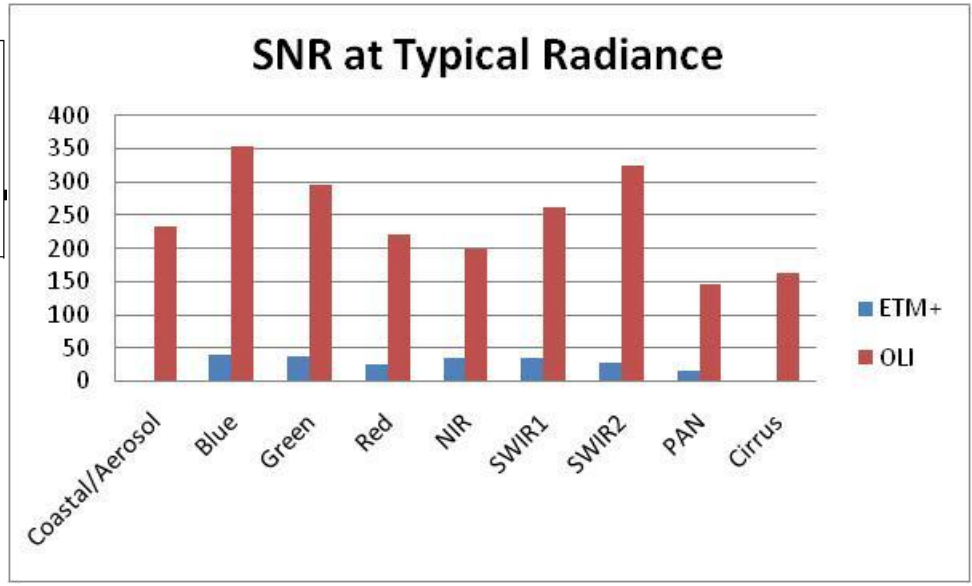

RSR have desired sharp bandpasses

Out-of-Band Response typically below 10^{-4}

Uniformity very good

SNR significantly exceeds requirements and heritage

LDCM Radiometric Performance Looks Excellent

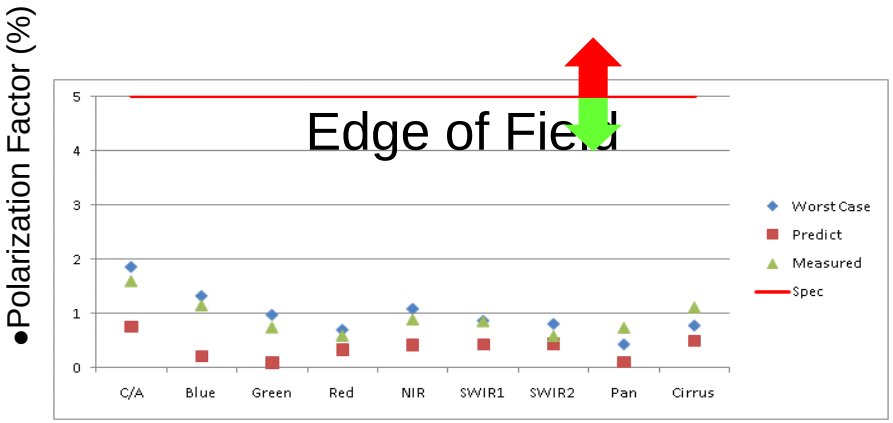

Polarization Sensitivity well below 2%

LDCM Data Collection Sequence

- The co-aligned sensors are nominally nadir pointed and sweep the ground track land surface in contiguous image data collections, also known as image intervals.
- The number of intervals are pre-defined on the ground based upon the number of WRS-2 scenes scheduled for collection, and allocated in the SSR.
- Each orbit will start and end with a 500 line dark collect (shutter closed)
- Each data collection sequence will start and end with an ancillary file

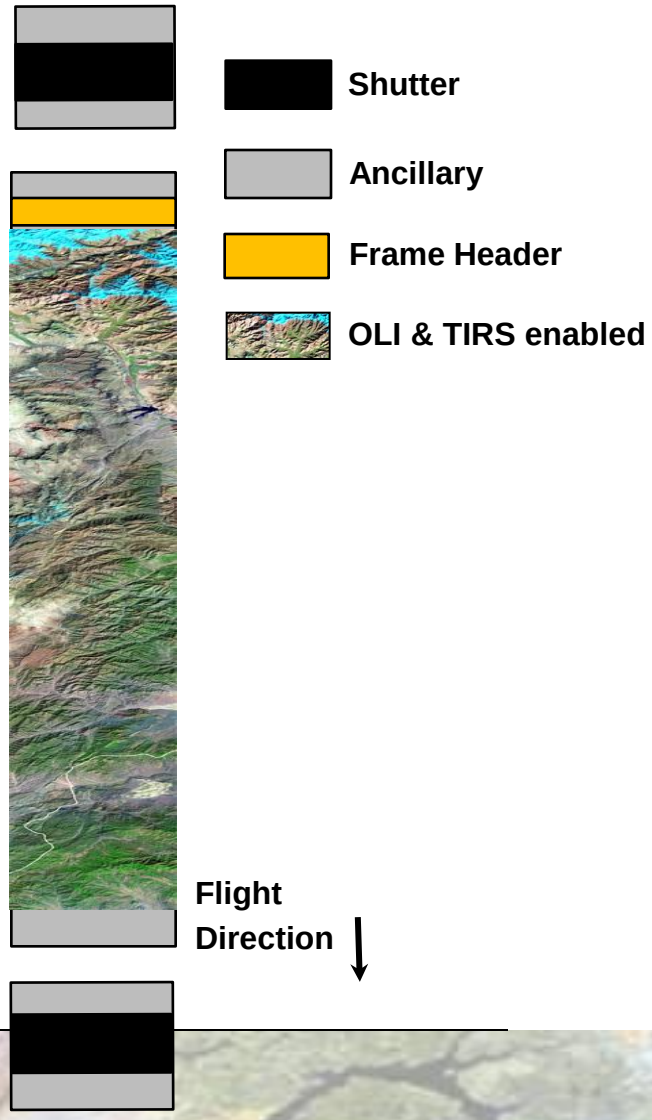

L8 Standard Level 1 Terrain Product

- **What will you receive?**
  - **LC82220052014265LGN00.tar.gz**
    - LC82220052014265LGN00_B1.TIF
    - LC82220052014265LGN00_B2.TIF
    - LC82220052014265LGN00_B3.TIF
    - LC82220052014265LGN00_B4.TIF
    - LC82220052014265LGN00_B5.TIF
    - LC82220052014265LGN00_B6.TIF
    - LC82220052014265LGN00_B7.TIF
    - LC82220052014265LGN00_B8.TIF
    - LC82210052014265LGN00_B9.TIF
    - LC82220052014265LGN00_B10.TIF
    - LC82220052014265LGN00_B11.TIF
    - LC82220052014265LGN00_QA.TIF
    - LC82220052014265LGN00_MTL.txt
- **With Checksum file LC82220052014265LGN00_MD5.txt**

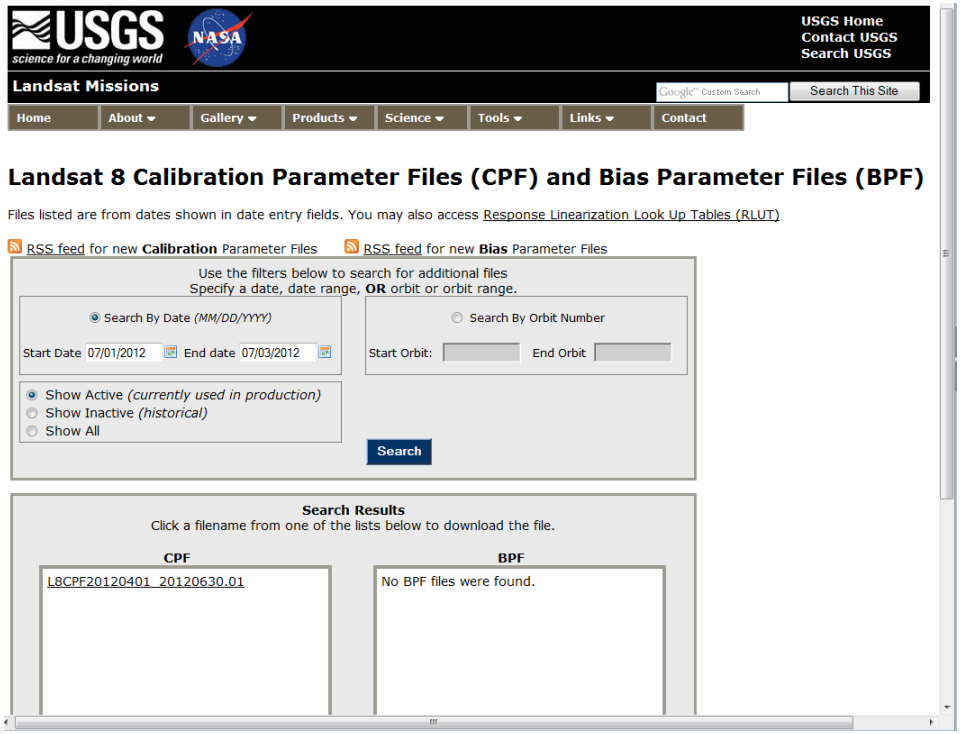

Quality Assessment Band A file that contains quality statistics from the image data and cloud mask for the scene

Bit	Description	Bit	Description
0	Designated Fill	8	Vegetation Confidence
1	Dropped Frame	9	
2	Terrain Occlusion	10	Snow/Ice Confidence
3	Artifact (Reserved)	11	
4	Water Confidence	12	Cirrus Confidence
5		13	
6	Cloud Shadow (reserved)	14	Cloud Confidence
7		15	

Bit	Description
0	Designated
1	Dropped Frame
2	Terrain Occlusion
3	Water**
4	Vegetation**
5	Snow/Ice**
6	Cirrus**
7	Cloud**

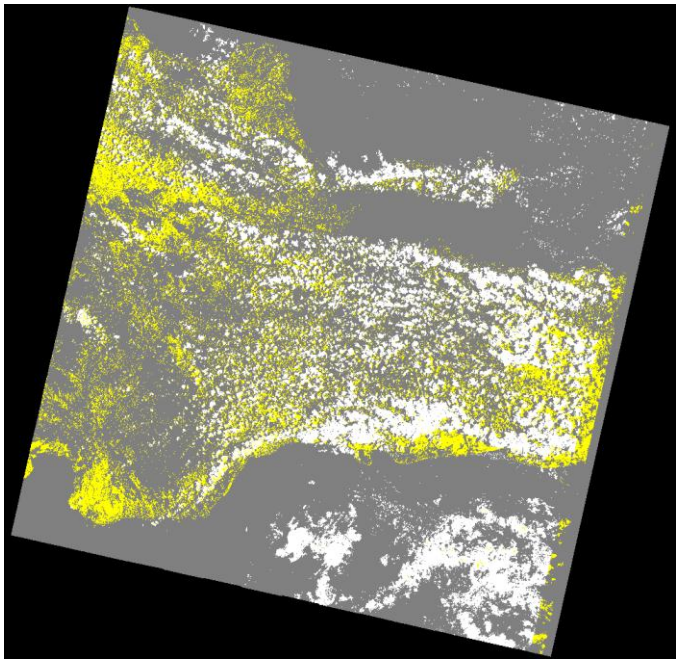

Quality Assessment Band (8-bit)

- 16-bit QB rolls off of the Online Cache with the L1 Product
- 8-bit QB available with the Full Resolution Browse

At-launch bits

**- Set for highest Confidence Level (11)

Confidence Levels
00 = none or unset
01 = 0-33% confidence
10 = 34-66% confidence
11 = 67-100% confidence

- The QB looks like any other band file and is a 16-bit image with the same dimensions as the L1T scene.
- The bits are assigned to various processing artifacts that are identified in the L1 processing.

LDCM L1 product options

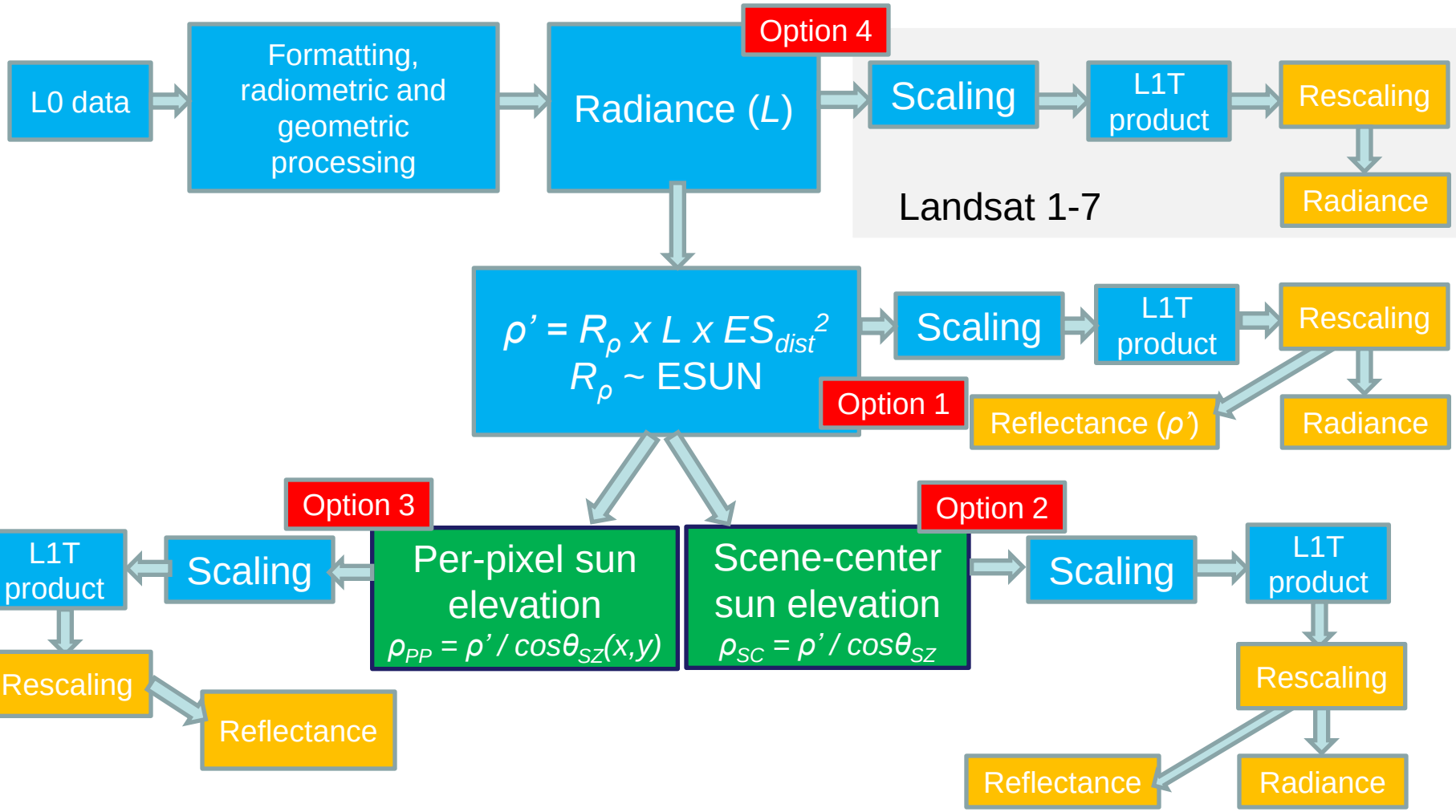

Test Site Catalog and Trending

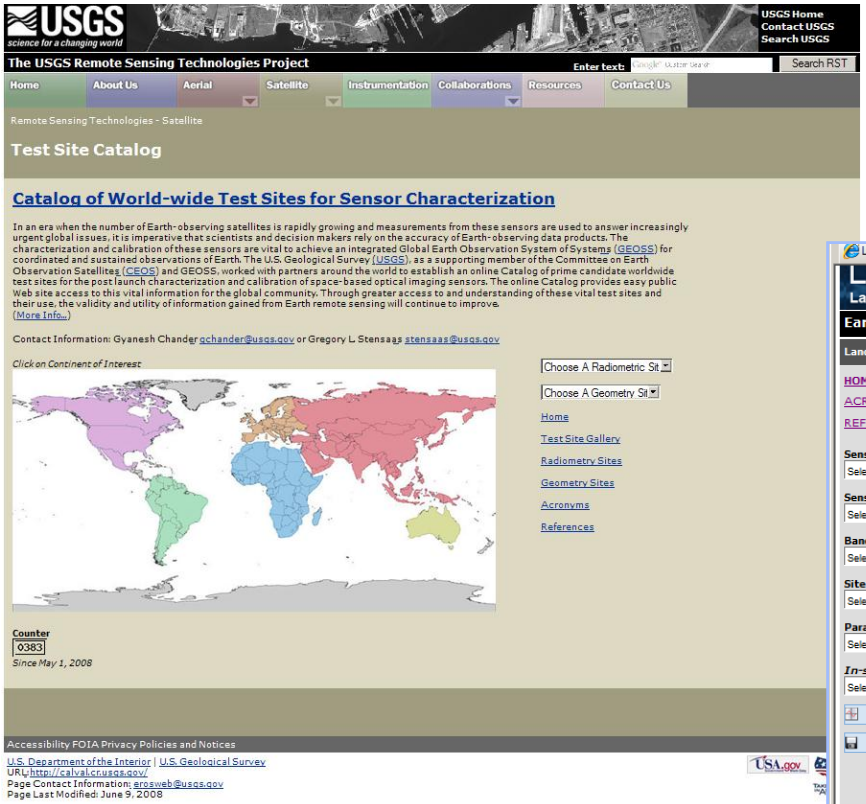

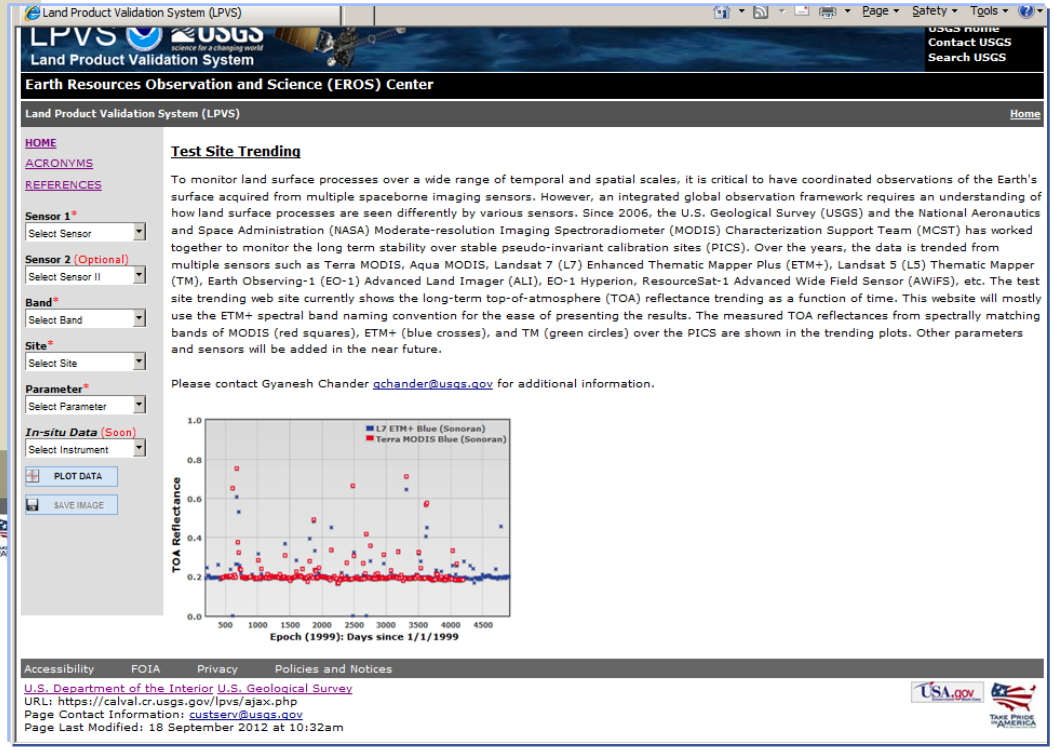

HOME
ACRONYMS
REFERENCES

Sensor 1*
Select Sensor

Sensor 2 (Optional)
Select Sensor II

Band*
Select Band

Site*
Select Site

Parameter*
Select Parameter

In-situ Data (Soon)
Select Instrument

PLOT DATA
SAVE IMAGE

Test Site Trending

To monitor land surface processes over a wide range of temporal and spatial scales, it is critical to have coordinated observations of the Earth's surface acquired from multiple spaceborne imaging sensors. However, an integrated global observation framework requires an understanding of how land surface processes are seen differently by various sensors. Since 2006, the U.S. Geological Survey (USGS) and the National Aeronautics and Space Administration (NASA) Moderate-resolution Imaging Spectroradiometer (MODIS) Characterization Support Team (MCST) has worked together to monitor the long term stability over stable pseudo-invariant calibration sites (PICS). Over the years, the data is trended from multiple sensors such as Terra MODIS, Aqua MODIS, Landsat 7 (L7) Enhanced Thematic Mapper Plus (ETM+), Landsat 5 (L5) Thematic Mapper (TM), Earth Observing-1 (EO-1) Advanced Land Imager (ALI), EO-1 Hyperion, ResourceSat-1 Advanced Wide Field Sensor (AWiFS), etc. The test site trending web site currently shows the long-term top-of-atmosphere (TOA) reflectance trending as a function of time. This website will mostly use the ETM+ spectral band naming convention for the ease of presenting the results. The measured TOA reflectances from spectrally matching bands of MODIS (red squares), ETM+ (blue crosses), and TM (green circles) over the PICS are shown in the trending plots. Other parameters and sensors will be added in the near future.

Please contact Gyanesh Chander gchander@usgs.gov for additional information.

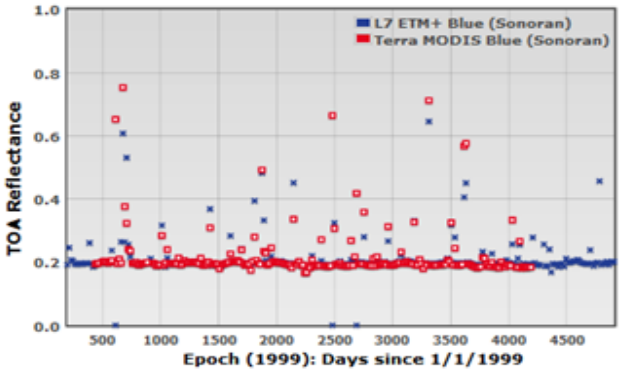

LPVS USGS science for a changing world
Land Product Validation System

Earth Resources Observation and Science (EROS) Center

Land Product Validation System (LPVS)

HOME
ACRONYMS
REFERENCES

Sensor 1*
L7 ETM+

Sensor 2 (Optional)
Select Sensor II

Band*
Blue

Site*
Libya 4

Parameter*
TOA Reflectance

In-situ Data (Soon)
Select Instrument

PLOT DATA

SAVE IMAGE

Data: series=1, x=1580.00, y=0.46

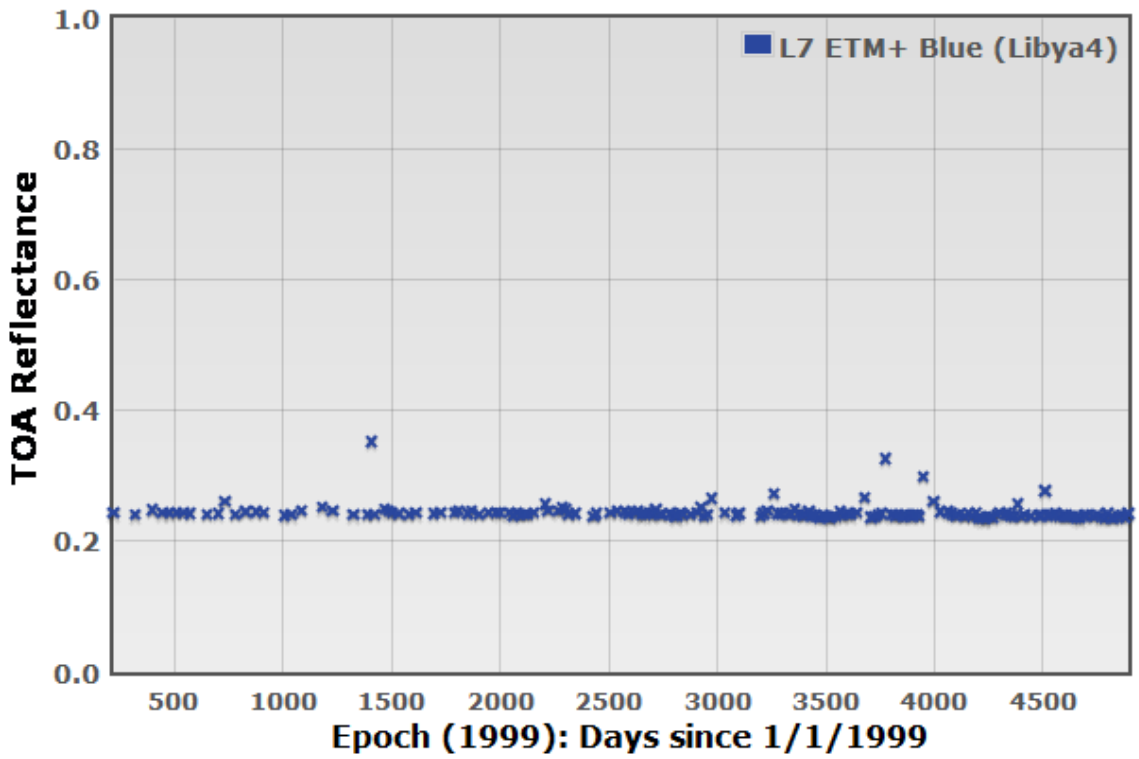

LPVS USGS science for a changing world
Land Product Validation System

Earth Resources Observation and Science (EROS) Center

Land Product Validation System (LPVS)

Sensor 1* L7 ETM+

Sensor 2 (Optional) Terra MODIS

Band* Blue

Site* Libya 4

Parameter* TOA Reflectance

In-situ Data (Soon) Select Instrument

PLOT DATA

SAVE IMAGE

Data: series=1, x=4860.00, y=0.24

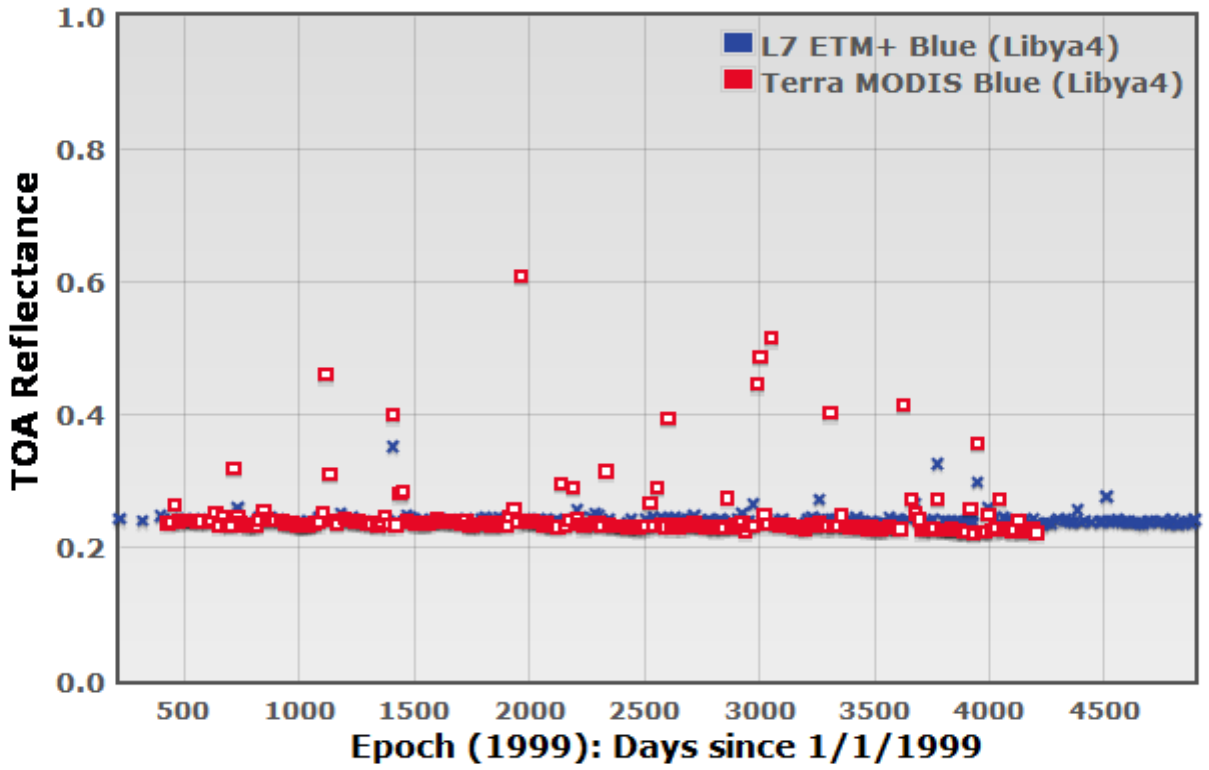

HOME
ACRONYMS
REFERENCES

Sensor 1*
L7 ETM+

Sensor 2 (Optional)
Select Sensor II

Band*
All Bands

Site*
Libya 4

Parameter*
TOA Reflectance

In-situ Data (Soon)
Select Instrument

PLOT DATA

SAVE IMAGE

Data: series=1, x=2316.00, y=0.24

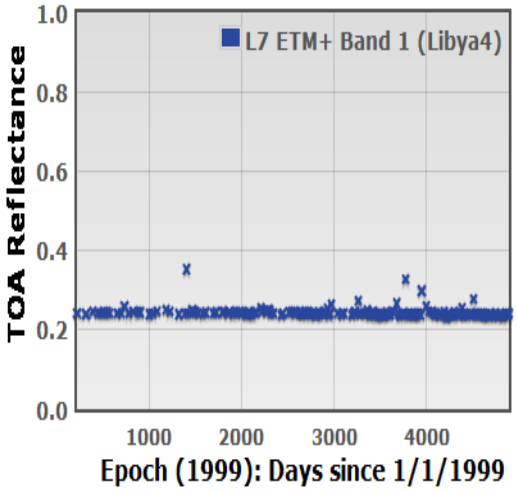

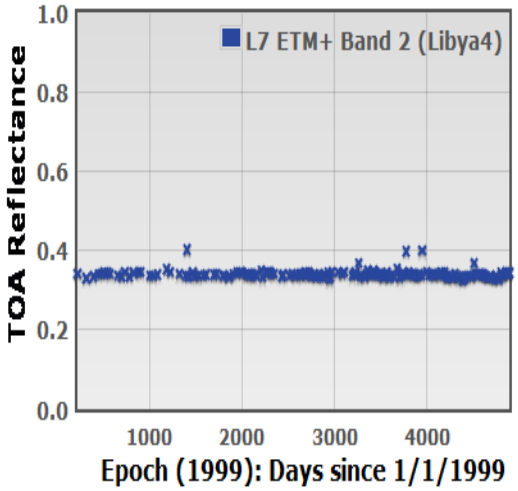

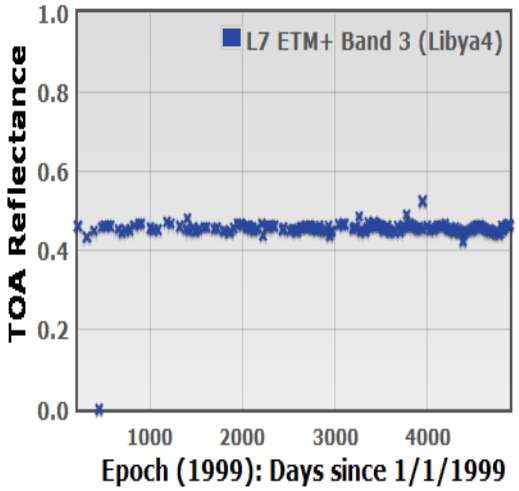

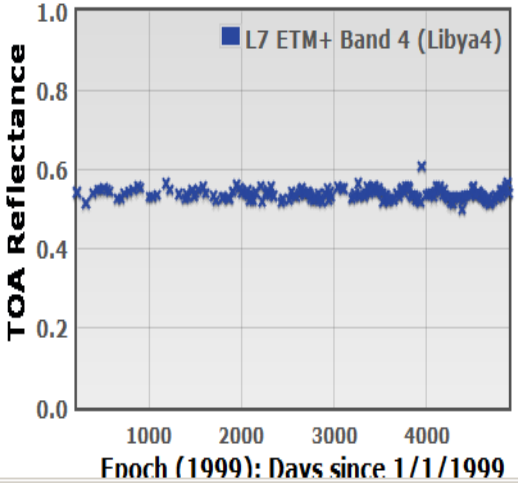

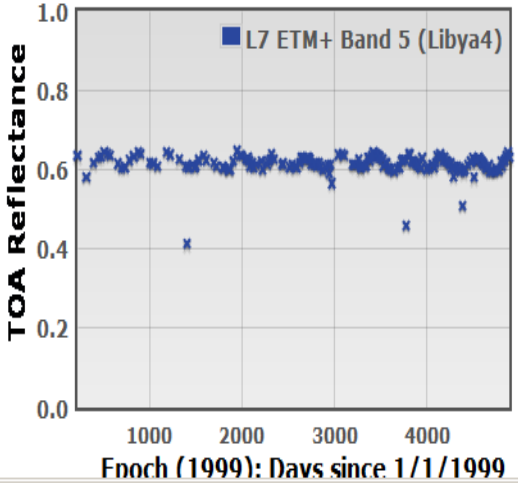

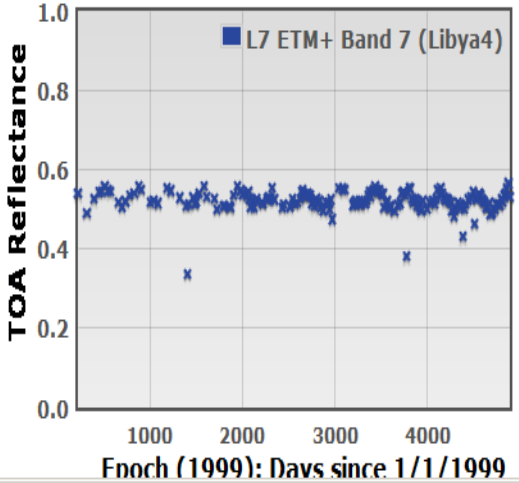

TOA ρ trending over the Libya 4 site

- Measured TOA ρ from MODIS (red squares) ETM+ (blue crosses)
- The slope of the fitted lines were ~10^{-7}/day, indicating very stable long-term response changing by no more than 0.02% per year (except B1) in their TOA reflectance
- Major contributions to offsets are caused by a combination of the spectral signature of the ROI, atmospheric composition, and the RSR of each sensor

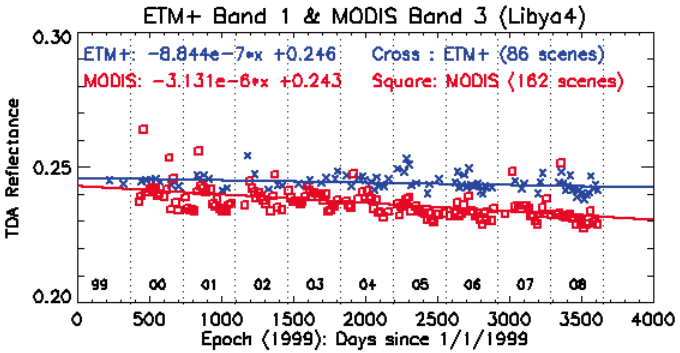

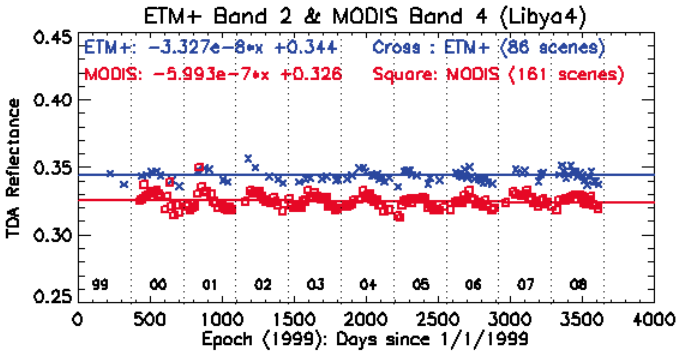

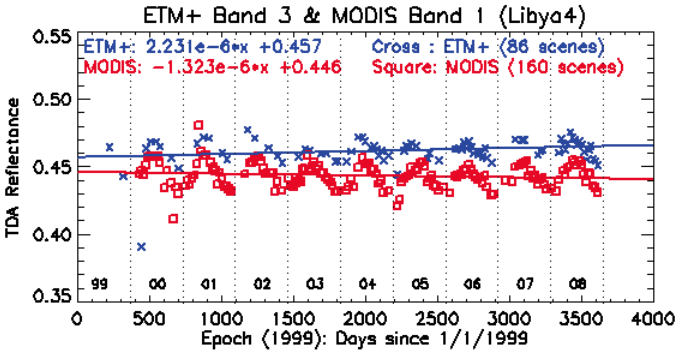

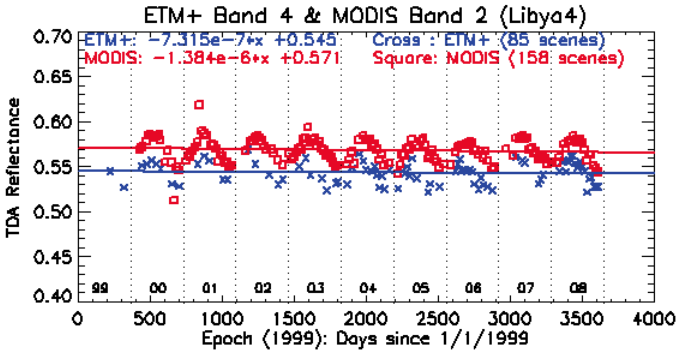

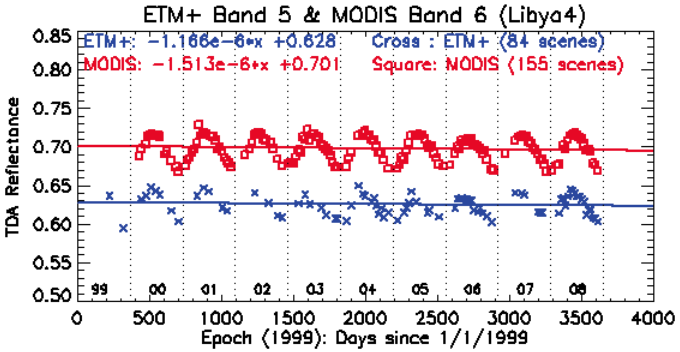

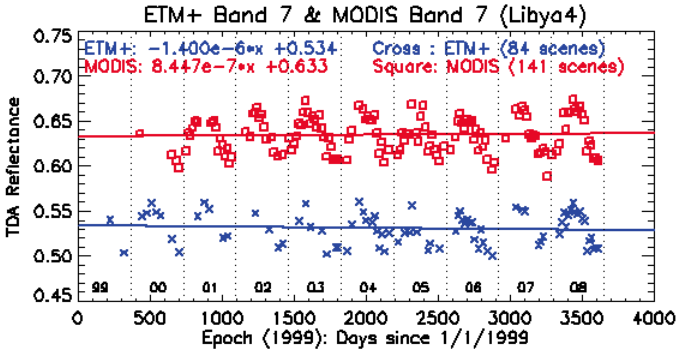

- The periodic seasonal oscillations in the TOA ρ trending is caused by the BRDF effects (while satellite zenith angle is nadir, the solar zenith angle varies significantly with season)

TOA ρ trending after SBAF compensation over the Libya 4 site

ETM+ Bands	1	2	3	4	5	7
% difference before SBAF	1.23%	5.52%	2.47%	-4.55%	-10.41%	-15.64%
% difference after SBAF	-5.51%	2.04%	-0.83%	4.06%	-5.42%	-3.18%

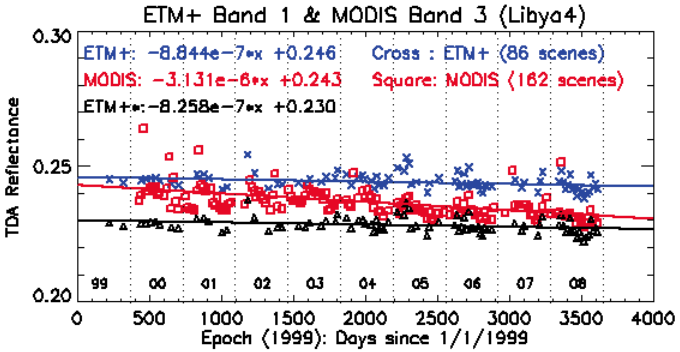

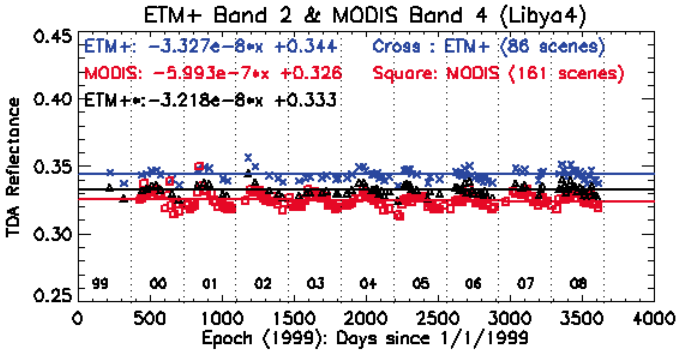

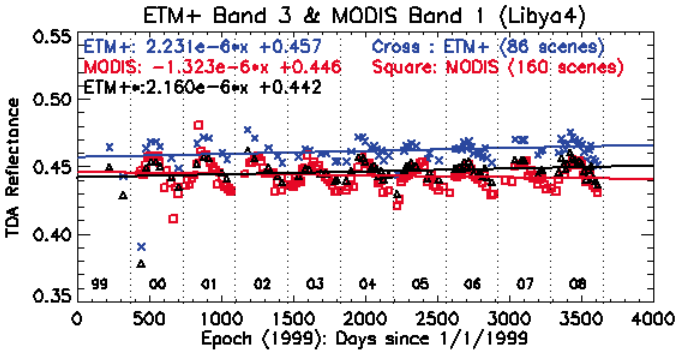

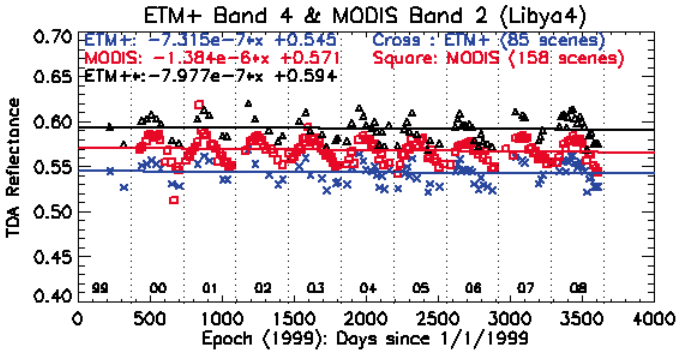

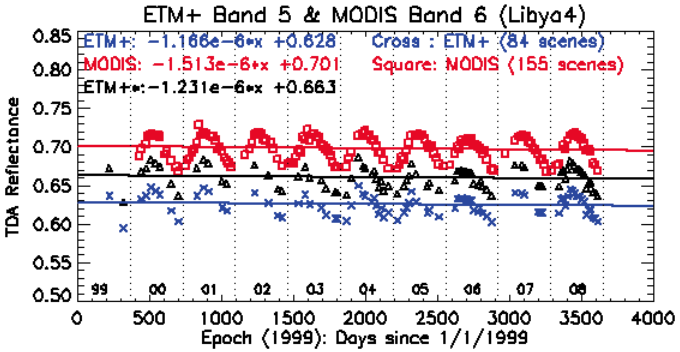

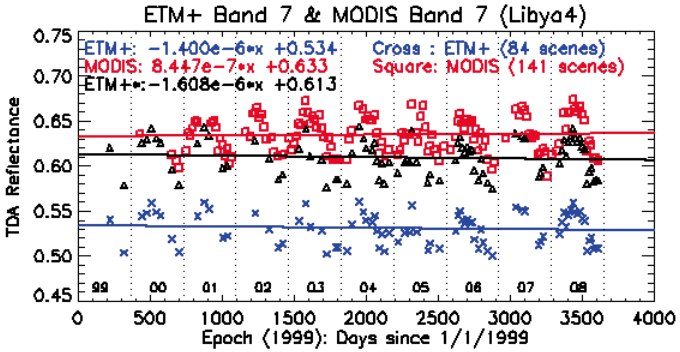

Metric for the CEOS Reference Pseudo-invariant Calibration Test Sites

Gyanesh Chander[a], Aisheng Wu[b], Xiaoxiong (Jack) Xiong[c], Amit Angal[d], Taeyoung (Jason) Choi[b], Dennis L. Helder[e]

[a] SGT, Inc*, U.S. Geological Survey (USGS) Earth Resources Observation and Science (EROS) Center, Sioux Falls, SD 57198 USA, Telephone: 605-594-2554, Email: gchander@usgs.gov *Work performed under USGS contract 08HQCN0005; [b]Sigma Space Corporation, 4400 Lottsford Vista Road, Lanham, Maryland 20706, USA; [c]NASA Goddard Space Flight Center (GSFC), Code 614.4, Greenbelt, MD 20771 USA; [d] Science Systems and Applications, Inc., 10210 Greenbelt Road, Suite 600, Lanham, MD 20706 USA; [e]South Dakota State University (SDSU), Brookings, SD, 57007, USA;

INTRODUCTION

➢ Test sites are central to future Earth Observation (EO) sensor data quality assurance and quality control (QA/QC) strategy.

➢The Committee on Earth Observation Satellites (CEOS) Working Group for Calibration and Validation (WGCV) Infrared Visible Optical Sensors (IVOS) worked with collaborators around the world to establish a core set of CEOS-endorsed, globally-distributed, reference standard test sites (both instrumented and pseudo-invariant) for the post-launch calibration of space-based optical imaging sensors.

➢The pseudo-invariant desert sites have high reflectance and are usually made up of sand dunes with low aerosol loading and, practically, no vegetation.

➢Consequently, these pseudo-invariant reference standard test sites can be used to evaluate the long-term stability of a sensor and to facilitate cross-comparison of multiple sensors.

➢The goal of this paper is to generate a metric for pseudo-invariant calibration test sites based on multiple parameters such as top-of-atmosphere (TOA) reflectance, at-sensor brightness temperature, spatial uniformity, temporal stability, data yield rate, usable area, spectral stability and typical spectrum observed over the site.

CEOS REFERNCE SITES

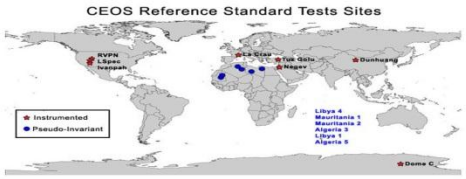

Fig. 1. Distribution of the CEOS reference standard test sites.

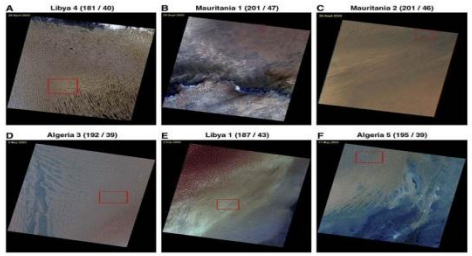

Fig. 2. Summary of the rectangular box region of interest (ROI) that were used within the Landsat 7 ETM+ images acquired over the CEOS reference standard pseudo-invariant desert test sites. The site name and the WRS-2 path and row information are also listed.

Table 1. ROI coordinates and dimension for the pseudo-invariant test sites.

Sites	WRS-2 Path/Row	Min_Lat	Min_Long	Max_Lat	Max_Long	UTM Zone	Area (km)
Libya 4	181 / 40	28.46	23.28	28.72	23.73	34	45 x 28
Mauritania 1	201 / 47	19.38	-9.47	19.58	-9.23	29	25 x 23
Mauritania 2	201 / 46	20.80	-8.82	20.97	-8.43	29	40 x 19
Algeria 3	192 / 39	30.22	7.46	30.42	7.86	32	39 x 22
Libya 1	187 / 43	24.33	13.20	24.51	13.57	33	37 x 20
Algeria 5	195 / 39	30.86	1.97	31.05	2.38	31	39 x 22

TOA REFLECTANCE PROFILE

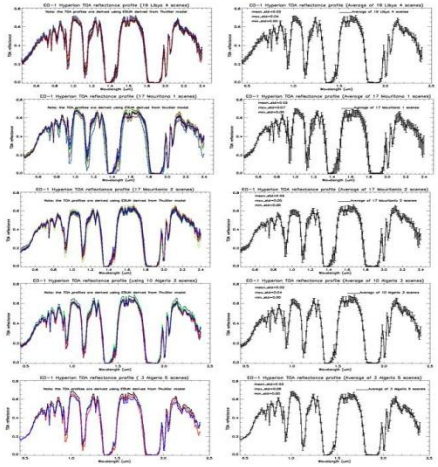

Fig. 3. Top-Of-Atmosphere (TOA) Reflectance Profile using EO-1 Hyperion data.

AVERAGE TOA REFLECTANCE

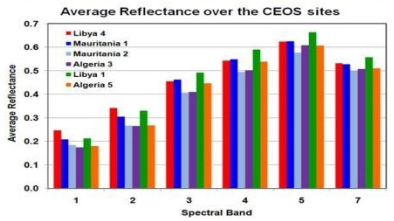

Fig. 4. Average TOA Reflectance is the multi-year average TOA reflectance for each band/site after removal of cloudy and anomalous images using L7 ETM+ data.

AVERAGE TEMPERATURE

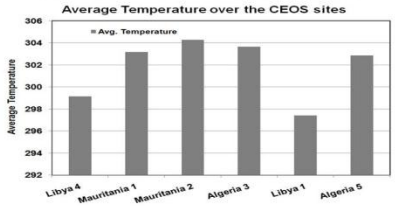

Fig. 5. Average brightness temperature is the multi-year average at-sensor temperature using L7 ETM+ data.

SPATIAL UNIFORMITY

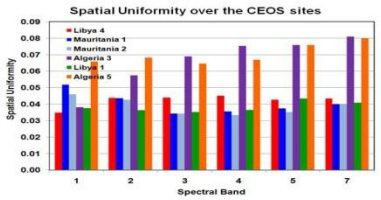

Fig. 6. Spatial uniformity is the multi-year average standard deviation/mean using L7 ETM+ data.

TEMPORAL STABILITY

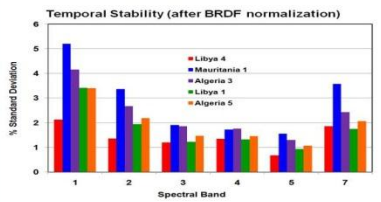

Fig. 7. Temporal Stability is the overall standard deviation of the average TOA reflectance over the lifetime using Terra MODIS data.

AVERAGE NDVI

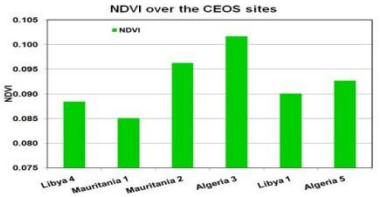

Fig. 8. Spectral multi-year average Normalized Difference Vegetation Index (NDVI) using L7 ETM+ data.

DATA YIELD RATE

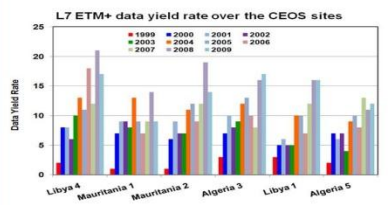

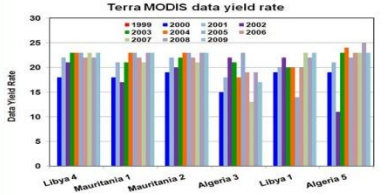

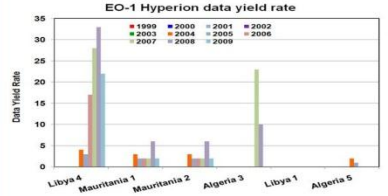

Fig. 9. Data yield rate is the number of nadir images (for ETM+ and MODIS) that are available in the archive over a given site.

SUMMARY

➢ The characterization and calibration of EO sensors, particularly their relative biases, are vital to achieve the developing integrated Global Earth Observation System of Systems (GEOSS) for coordinated and sustained observations of the Earth.

➢This can only reliably be achieved in the post-launch environment through the careful use of observations by multiple sensor systems over common, well-characterized terrestrial targets.

➢ L7 ETM+, EO-1 Hyperion and Terra MODIS TOA measurements were used to derive all the metrics which will enable us to evaluate the differences between all the sites.

➢ Comparison between the pseudo-invariant sites has been performed using multiple parameters such as TOA reflectance, at-sensor brightness temperature, spatial uniformity, spectral and temporal stability, data yield rate.

➢ All the six pseudo-invariant desert sites exhibit relatively high TOA reflectance along with a high data yield rate.

➢In general, the widely used Libya 4 site exhibit the best performance amongst the sites under consideration in terms of temporal stability, spatial uniformity and high data yield rate (EO-1 Hyperion and L7 ETM+).

➢Additional work is underway to characterize the multiple parameters and define a single figure of merit.

Use of EO-1 Hyperion Data to Calculate Spectral Band Adjustment Factors (SBAF) between the L7 ETM+ and Terra MODIS Sensors

G. Chander[a], N. Mishra[b], D. L. Helder[b], D. Aaron[b], T. Choi[c], A. Angal[d], X. Xiong[e]

[a]SGT, Inc., contractor to the U.S. Geological Survey (USGS) Earth Resources Observation and Science (EROS) Center, Sioux Falls, SD, 57198, USA. Work performed under U.S. Geological Survey contract 08HQCN0005. Telephone: 605-594-2554, Email: gchander@usgs.gov.[b]South Dakota State University (SDSU), Brookings, SD, 57007, USA. [c]Sigma Space Corporation, 10210 Greenbelt Road, Lanham, MD, 20706, USA. [d]Science Systems and Applications (SSAI), Inc., 10210 Greenbelt Road, Lanham, MD, 20706, USA. [e]National Aeronautics and Space Administration (NASA) Goddard Space Flight Center (GSFC), Greenbelt, MD, 20771, USA.

1. INTRODUCTION

- In this study, spectral band adjustment factors (SBAF) are derived using hyperspectral Earth Observing-1 (EO-1) Hyperion measurements to adjust for the spectral band differences between the Landsat 7 (L7) Enhanced Thematic Mapper Plus (ETM+) and the Terra Moderate Resolution Imaging Spectroradiometer (MODIS) top-of-atmosphere (TOA) reflectance measurements from 2000 to 2009 over the pseudo-invariant Libya 4 reference standard test site
- The motivation of the work comes from the need to adjust the spectral response differences of multispectral sensors in order to provide more accurate cross-calibration between the sensors.

2. METHODOLOGY

- In this study, the Libya 4 TOA reflectance profile was generated using an average of 108 cloud-free images from 2004 to 2009 acquired using the EO-1 Hyperion sensor.
- Fig. 1 illustrates an average Libya 4 spectral TOA reflectance profile from Hyperion (average of 108) plotted along with the RSR profiles of the ETM+ and MODIS sensors.
- The SBAF was calculated by convolving the spectral response of the ETM+ and MODIS sensors with the Hyperion TOA reflectance profile at each sampled wavelength, weighted by the respective RSR
- To adjust TOA reflectance data for sensor spectral response differences, the following equations were used.

$$\bar{\rho}_{sensor} = \frac{\int \rho_\lambda RSR_\lambda d\lambda}{\int RSR_\lambda d\lambda} \quad (1)$$

$$SBAF = \frac{\bar{\rho}_{ETM+}}{\bar{\rho}_{MODIS}} = \frac{\left(\int \rho_\lambda RSR_{\lambda ETM+} d\lambda\right) / \left(\int RSR_{\lambda ETM+} d\lambda\right)}{\left(\int \rho_\lambda RSR_{\lambda MODIS} d\lambda\right) / \left(\int RSR_{\lambda MODIS} d\lambda\right)} \quad (2)$$

$$\bar{\rho}^*_{MODIS} = \bar{\rho}_{ETM+} / SBAF \quad (3)$$

where
RSR_λ = Relative Spectral Response of the sensor [unitless]
ρ_λ = Hyperspectral TOA reflectance profile generated from the EO-1 Hyperion [unitless]
$\bar{\rho}_{ETM+}$ = Simulated ETM+ TOA reflectance generated using the EO-1 Hyperion profile [unitless]
$\bar{\rho}_{MODIS}$ = Simulated MODIS TOA reflectance generated using the EO-1 Hyperion profile [unitless]
$\bar{\rho}^*_{MODIS}$ = Adjusted ETM+ reflectance using the SBAF to match the MODIS reflectance [unitless]

- Hyperion has a spectral resolution of 10 nm, and the spectral sampling intervals of the ETM+ and MODIS RSRs is 1 nm
- To understand the effects of interpolation, SBAFs were generated using spline, quadratic, and least square (LS) quadratic interpolation.
- The analysis showed that the change in SBAF due to interpolation techniques is less than 0.2% for all bands (Table I).

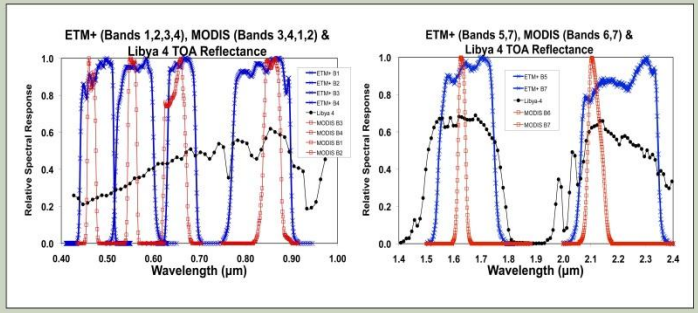

Figure 1. Comparison of the Libya 4 TOA reflectance profile and the RSR profiles from the ETM+ and MODIS sensors.

Table 1. Variations in SBAF due to interpolation.

ETM+ Bands	Spline	Quadratic	LS Quadratic	Average	STD of three INT methods
1	1.065	1.069	1.066	1.067	0.19%
2	1.033	1.033	1.034	1.033	0.10%
3	1.035	1.035	1.035	1.035	0.03%
4	0.915	0.914	0.916	0.915	0.08%
5	0.948	0.949	0.947	0.948	0.06%
7	0.869	0.870	0.870	0.870	0.05%

- 108 Hyperion images acquired over five years from 2004 to 2009 were processed to obtain the average TOA reflectance profiles.
- The standard deviations of all those profiles were lower than 0.05 for all Hyperion bands.
- The minimum, maximum, and average SBAF, and their standard deviation (STD) are provided in Table II.
- The average of the band-dependent SBAF was used to adjust the lifetime ETM+ TOA reflectance to match with MODIS TOA reflectance.

Table 2. Hyperion-derived SBAF from Libya 4.

ETM+ Bands	ρ_{ETM+}	ρ_{MODIS}	SBAF Average	SBAF Max	SBAF Min	RMSE	STD of 108 SBAF
1	0.244	0.228	1.066	1.0763	1.0434	2.34%	0.82%
2	0.348	0.337	1.034	1.0416	1.0231	1.29%	0.38%
3	0.470	0.454	1.035	1.0445	1.0318	0.96%	0.32%
4	0.542	0.591	0.916	0.9324	0.8964	2.79%	0.77%
5	0.638	0.674	0.947	0.9681	0.925	3.22%	0.91%
7	0.530	0.609	0.870	0.8811	0.8543	2.20%	0.58%

3. RESULTS AND DISCUSSIONS

Fig. 2 shows the long-term TOA reflectance trending of the spectrally matching bands of the ETM+ and MODIS sensors over the Libya 4 site.

- The measured TOA reflectances from MODIS (red squares) and ETM+ (blue crosses) have been trended for the Libya 4 site and the SBAF-adjusted ETM+ reflectances (black squares) are also shown.
- These constant offsets between the two sensors are likely caused by a combination of the spectral signature of the target, atmospheric composition, and the RSR characteristics of each sensor. In an effort to minimize the effect of change in environment, same-day Hyperion, ETM+, and MODIS images were selected for SBAF adjustment.
- The percentage difference between the ETM+ and MODIS TOA reflectances over the lifetime [before and after SBAF adjustments] are summarized in table III.

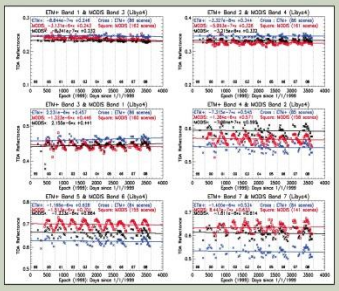

Figure 2. TOA reflectance trending over the Libya 4 site.

Table 3. Effects of SBAF on Lifetime Libya-4 Data.

ETM+ Bands	TOA ρ_{ETM+}	TOA ρ_{MODIS}	TOA ρ_{MODIS^*}	% difference (E-M)/M% before SBAF	% difference (M*-M)/M% after SBAF
1	0.246	0.243	0.232	1.23%	-4.53%
2	0.344	0.326	0.332	5.52%	1.84%
3	0.457	0.446	0.441	2.47%	-1.12%
4	0.545	0.571	0.595	-4.55%	4.20%
5	0.628	0.701	0.664	-10.41%	-5.28%
7	0.534	0.633	0.614	-15.64%	-3.00%

- 10 same-day images were processed and the corresponding day specific SBAF adjustment was applied as described earlier.
- The average (of 10 image pairs) percentage difference between ETM+ and MODIS TOA reflectances using same-day images are provided in Table IV.
- The improvements noted in Band 1 reinforce the concept that changes in Rayleigh scattering over the large time intervals in the 108 data point set may have caused the problems with the generalized SBAF correction for this band.
- Another source of uncertainty in the SBAF adjustment can arise due to filter spectral uncertainties.
- The spectral uncertainty of ETM+ was not available.

Table 4. Effect of SBAF on Same-Day Libya-4 Data.

ETM+ Bands	% difference (E-M)/M% before SBAF	% difference (M*-M)/M% after SBAF
1	4.68%	-1.93%
2	5.63%	2.08%
3	4.31%	-0.92%
4	4.31%	4.28%
5	-10.54%	-5.53%
7	-16.24%	-3.21%

- With the spectral uncertainties for each band known, the SBAF were calculated for both positive and negative spectral shifts of the Hyperion and MODIS bands.
- The directions of spectral shifts, the uncertainties due to these spectral shifts, and RMSE values for each band are summarized in Table V.
- These RMSE values were used as an estimation of the net uncertainty in SBAF adjustment due to filter spectral uncertainties.
- The aim of this exercise was to quantify the uncertainties in the SBAF adjustment resulting from the spectral uncertainties of the sensors being used.

Table 5. Variations in SBAF due to spectral uncertainties in MODIS and Hyperion RSR.

ETM+ Bands	Hyperion [-] Shift	Hyperion [+] Shift	MODIS [-] Shift	MODIS [+] Shift	MODIS [+] & Hyperion [-] Shift	MODIS [-] & Hyperion [+] Shift	MODIS [-] & Hyperion [-] Shift	MODIS [+] & Hyperion [+] Shift	RMSE
1	0.00%	0.07%	1.20%	0.83%	1.19%	0.42%	2.13%	0.74%	2.10%
2	0.07%	0.40%	0.89%	1.02%	1.19%	0.53%	1.45%	0.28%	2.53%
3	0.29%	0.22%	0.24%	0.33%	0.73%	0.46%	0.23%	0.06%	0.98%
4	0.48%	0.02%	0.86%	0.86%	1.32%	0.27%	1.66%	0.19%	2.63%
5	0.24%	0.46%	1.60%	0.66%	0.85%	0.46%	3.33%	0.96%	5.25%
7	0.58%	1.25%	0.66%	2.09%	0.26%	0.94%	2.93%	2.57%	4.46%

4. CONCLUSION

- This paper demonstrates the use of EO-1 Hyperion data to adjust for the spectral band differences between ETM+ and MODIS sensors over Libya 4.
- Before SBAF adjustment, ETM+ TOA reflectance was lower than 16% of MODIS TOA reflectance for all the bands. After spectral adjustment, the RSR-adjusted ETM+ TOA reflectance (MODIS*) measurements agree with MODIS lower than 6% for all bands.
- The TOA reflectance adjustment from Bands 1, 4, and 5 were unsatisfactory: Band 1 is strongly influenced by Rayleigh scattering, the over-adjustment in Band 4 was attributed to water vapor absorption feature, and the inadequate adjustment for Band 5 can be attributed to water vapor because of its close proximity to the absorption feature at 1800 nm.
- The uncertainty analysis in the SBAF due to change in Hyperion acquisition date, change in atmosphere, and shifts in spectral responses were performed.
- Higher uncertainties were observed in Bands 1, 4, and 5. These higher uncertainties were consistent with results from these three bands giving higher percentage differences after SBAF adjustment.
- Additional research needs to be done to reduce the disagreement in the results at longer wavelengths, and the role of atmosphere in the SBAF estimation needs to be further studied.

USGS
science for a changing world

Radiometric Cross-calibration of EO-1 ALI with L7 ETM+ and Terra MODIS Sensors

Gyanesh Chander

SGT, Inc., contractor to the U.S. Geological Survey (USGS) Earth Resources Observation and Science (EROS) Center, Sioux Falls, SD, 57198, USA.

Work performed under USGS contract G10PC00044. Telephone: 605-594-2554, Email: gchander@usgs.gov.

Introduction

- The Earth Observing-1 (EO-1) satellite was launched on November 21, 2000, as part of a one-year technology demonstration mission but was extended because of the scientific communities interest
- To evaluate the Advanced Land Imager (ALI) sensor capabilities as a precursor to Operational Land Imager (OLI) onboard Landsat Data Continuity Mission (LDCM, or Landsat 8) , its measured top-of-atmosphere (TOA) reflectances were compared to the well-calibrated Landsat 7 (L7) Enhanced Thematic Mapper Plus (ETM+) and the Terra Moderate Resolution Imaging Spectroradiometer (MODIS) sensors in the reflective solar bands (RSB)
- The cross-calibration of ALI with ETM+ and MODIS was performed using near-simultaneous surface observations based on image statistics from areas observed by these sensors over four Desert sites (Libya 4, Mauritania 2, Arabia 1, and Sudan 1)
- The differences in the measured TOA reflectances due to Relative Spectral Response (RSR) mismatches were compensated by using a spectral band adjustment factor (SBAF), which takes into account the spectral profile of the target and the RSR of each sensor

Sensor Overview and Study Area

Table 1. ALI, ETM+, AND MODIS key specifications

Platform	EO-1	Landsat 7	Terra
Sensor	ALI	ETM+	MODIS
Launch date	November 21, 2000	April 15, 1999	December 18, 1999
Number of bands	10	8	36
Spatial resolution	10 m, 30 m	15 m, 30 m, 60 m	250 m, 500 m, 1 km
Swath	37 km	185 km	2330 km
Spectral coverage	0.4 – 2.5 µm	0.4 – 12.5 µm	0.4 – 14 µm
Pixel quantization	12 bit	8 bit	12 bit
Orbit type	Sun-synchronous	Sun-synchronous	Sun-synchronous
Equatorial Crossing Time	10:01 AM	10:00 AM	10:30 AM
Altitude	705 km	705 km	705 km
Repeat Cycle	16 days	16 days	1 – 2 days

•Recently, the Committee on Earth Observation Satellites (CEOS) Working Group on Calibration and Validation (WGCV) members of the Infrared Visible Optical Sensors (IVOS) sub-group has established a set of CEOS reference standard test sites for the post-launch calibration of space-based optical imaging sensors

•The six CEOS reference Pseudo Invariant Calibration Sites (PICS) are Libya 4, Mauritania 1, Mauritania 2, Algeria 3, Libya 1, and Algeria 5

•Due to the limited availability of ALI and Hyperion images over the CEOS PICS, only the following four sites were chosen in this study: Libya 4, Mauritania 2, Arabia 1, and Sudan 1

Table 2. ALI, ETM+, MODIS, AND HYPERION images used for the study

Site Name	WRS-2 Path/Row	ALI	ETM+	MODIS	Hyperion	ALI/ETM+/MODIS Same-Day Pairs
Libya 4	181 / 40	252	156	261	250	28
Mauritania 2	201 / 46	102	133	261	92	10
Arabia 1	165 / 47	157	161	220	155	22
Sudan 1	177 / 45	113	163	261	114	17

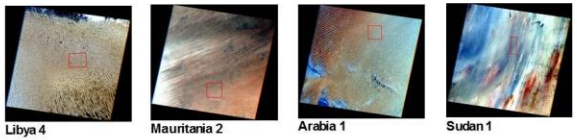

Fig. 1. A sample image of the four PICS acquired using L7 ETM+ (note that the scales differ). It also illustrates the rectangular region of interest (ROI) that were used within the image-pairs.

Spectral Band Adjustment Factor (SBAF)

- The difference in the spectral bands between the two sensors introduces an intrinsic offset in the measured TOA reflectances
- A target ROI specific SBAF, which takes into account the spectral profile of the target and the RSR of the two sensors, can be used to compensate for this difference. The simulated reflectance for any sensor can be calculated by integrating the spectral response of the sensor with the hyperspectral TOA reflectance profile at each sampled wavelength, weighted by the respective RSR (equation 1)
- The integral in the numerator calculates the amount of in-band reflectance acquired in the respective RSR and is divided by the integral of the RSR of the sensor so there is no gain/loss due to the filter response function
- The SBAF is then calculated by integrating the spectral response of sensor A and B with the hyperspectral TOA reflectance profile at each sampled wavelength, weighted by the respective RSR as described above
- Therefore, the ratio of the two simulated reflectances gives a quantitative estimate of the difference between the observed reflectance of the two sensors arising from mismatching RSR for a given band and target

$$\overline{\rho}_{\lambda(A)} = \frac{\int \rho_\lambda \, RSR_\lambda \, d\lambda}{\int RSR_\lambda \, d\lambda}$$

$$SBAF = \frac{\overline{\rho}_{\lambda(A)}}{\overline{\rho}_{\lambda(B)}} = \frac{\left(\int \rho_\lambda \, RSR_{\lambda(A)} d\lambda\right) / \left(\int RSR_{\lambda(A)} d\lambda\right)}{\left(\int \rho_\lambda \, RSR_{\lambda(B)} d\lambda\right) / \left(\int RSR_{\lambda(B)} d\lambda\right)}$$

$$\overline{\rho}^{*}_{\lambda(A)} = \overline{\rho}_{\lambda(A)} / SBAF$$

where

- RSR_λ = Relative Spectral Response of the sensor [unitless]
- ρ_λ = Hyperspectral TOA reflectance profile [unitless]
- $\overline{\rho}_{\lambda(A)}$ = Simulated TOA reflectance for sensor A [unitless]
- $\overline{\rho}_{\lambda(B)}$ = Simulated TOA reflectance for sensor B [unitless]
- $\overline{\rho}^{*}_{\lambda(A)}$ = Compensated TOA reflectance for sensor A using the SBAF to match sensor B TOA reflectance [unitless]

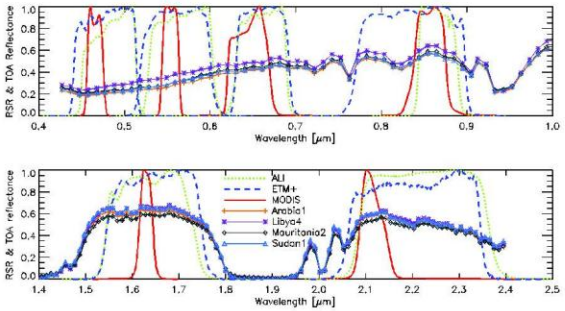

Fig. 2. Comparison of RSR profiles from the ALI, ETM+, and MODIS sensors along with the lifetime average EO-1 Hyperion TOA reflectance profile obtained for the four sites.

Results

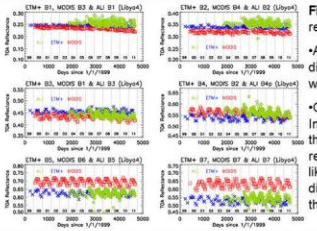

Fig. 3. ALI, ETM+, and MODIS measured TOA reflectance trending over the Libya 4 site

•ALI TOA reflectance is denoted with green diamonds, ETM+ with blue crosses, and MODIS with red squares

•Overall, the long-term trends are extremely stable. In addition to the possible calibration bias between these sensors, the offset between the TOA reflectance trends of ALI, ETM+, and MODIS are likely caused by a combination of the RSR differences, spectral signature of the target, and the atmospheric composition during overpass

Fig. 4. Measured TOA reflectance ratio (ETM+/ALI) over the four PICS. The plot also shows a comparison of before and after SBAF compensation.

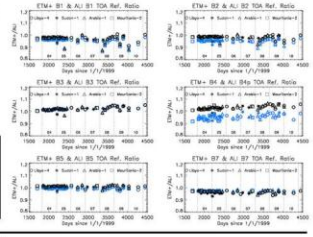

Table 3. Comparison of the ALI and ETM+ measured TOA reflectances before and after spectral compensation.

ETM+ Band	ρETM+ALI Average	% difference (B-A)/A%	ρETM+ALI STD	ρETM+ALI Average	% difference (B*-A)/A%	ρETM+ALI STD	% difference (B5-A5)/A5%
	Before SBAF			After SBAF			
1	0.994	-0.59%	0.024	0.971	-2.92%	0.025	-1.62%
2	0.953	-4.70%	0.015	0.981	-1.90%	0.015	-0.85%
3	1.019	1.90%	0.015	1.026	2.55%	0.015	4.15%
4	0.956	-4.40%	0.015	1.032	3.20%	0.015	-7.36%
5	0.994	0.00%	0.009	1.004	0.89%	0.009	1.39%
7	0.968	-3.26%	0.011	0.984	-1.93%	0.010	0.41%

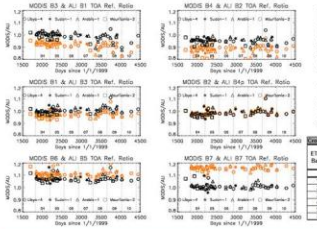

Fig. 5. Measured TOA reflectance ratio (MODIS/ALI) over the four PICS. The plot also shows a comparison of before and after SBAF compensation

Table 4. Comparison of the ALI and MODIS measured TOA reflectances before and after spectral compensation.

ETM+ Band	ρMODISALI Average	% difference (B-A)/A%	ρMODISALI STD	ρMODISALI Average	% difference (B*-A)/A%	ρMODISALI STD	% difference (B5-A5)/A5%
	Before SBAF (B5)			After SBAF (B5)			
1	0.919	-8.10%	0.030	0.956	-1.99%	0.032	-1.31%
2	0.882	-11.89%	0.031	0.954	-4.69%	0.024	-7.55%
3	0.971	-3.56%	0.023	1.006	0.68%	0.023	0.48%
4	0.990	-1.05%	0.025	0.996	-1.40%	0.024	0.41%
5	1.111	11.10%	0.026	1.070	7.28%	0.024	3.64%
7	1.162	16.35%	0.026	1.019	1.08%	0.024	15.05%

Summary

- This study summarizes the cross-calibration of ALI, ETM+, and MODIS sensors on the "A.M. constellation" train and explores the impact of spectral compensation on the data.
- All the near-simultaneous mages over Libya 4, Mauritania 2, Arabia 1, and Sudan 1 were selected over the mission's lifetime to perform cross-calibration between the three sensors.
- Spectral issues with this cross-calibration approach were investigated and SBAFs were developed for analogous spectral bands where the spectral signature of the target was simulated using EO-1 Hyperion data.
- The cross-calibration results showed the ALI agrees with ETM+ within 4%. Since the RSR of these two sensors are very similar, the spectral compensation did not alter the results much.
- However, due to large differences in the RSR between ALI and MODIS, the spectral compensation resulted in significant improvement in the cross-calibration between ALI and MODIS. The results show that the ALI agrees with MODIS within 5% (except Band 5).

Acknowledgement

The author appreciates the continued support of the NASA MODIS Characterization Support Team (MCST) and South Dakota State University (SDSU) Image Processing Laboratory team members. Any use of trade, product, or firm names is for descriptive purpose only and does not imply endorsement by the U.S. government.

Evaluation and Comparison of the IRS-P6 AWiFS and the Landsat Sensors

Gyanesh Chander[1], Dennis L. Helder[2], Thomas R. Loveland[3], Gregory L. Stensaas[3], Brian L. Markham[4], James R. Irons[4]

[1]SGT, Inc., contractor to the U.S. Geological Survey (USGS) Earth Resources Observation and Science (EROS) Center, Sioux Falls, SD. Work performed under USGS contract 08HQCN0005.
[2]South Dakota State University, [3]USGS EROS, [4]NASA Goddard Space Flight Center

Overview

- Need for Cross-calibration
  - Tie similar & differing sensors onto a common radiometric scale
  - Provide mission continuity, interoperability, and data fusion
  - Essential where on-board references are not available or where vicarious calibration is not feasible
  - Critical to coordinate observations from different sensors, exploiting their individual spatial resolutions, temporal sampling, and information content to monitor surface processes

RSR Comparison

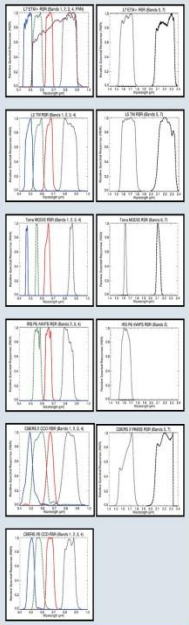

Catalog of Worldwide Test Sites

Cross-Calibration Methodology

- Co-incident image pairs from the two sensors were compared
- The cross-cal was performed using image statistics from large common areas observed by the two sensors
  - Define Regions of Interest over identical homogenous regions
    - All ROIs have about 400 x 400 Landsat pixels (160000 points) and 214 x 214 AWiFS pixels (45796 points)
    - Bright and dark regions were selected to obtain a maximum coverage over each sensor's dynamic range
    - All the saturated pixels and SLC-off pixels were discarded
  - Calculated the mean and standard deviation of the ROIs
  - Converted the satellite DN to TOA reflectance
- Performed a linear fit between the satellites to calculate the cross-cal gain and bias

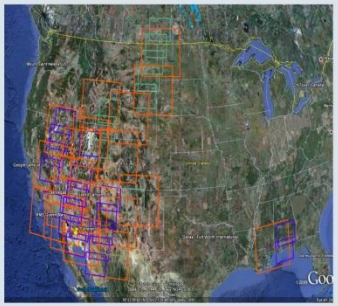

L5 TM, L7 ETM+ & P6 AWiFS Image Pairs

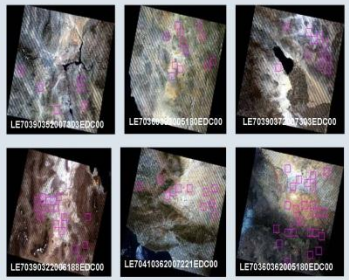

Areas in common between the L7 ETM+ and the P6 AWiFS (BD-quads) image pairs. The illustration shows the ETM+ images.

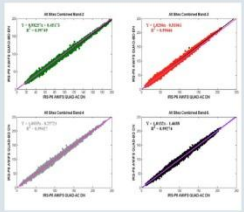

AWiFS Dual Camera Radiometric Consistency Check

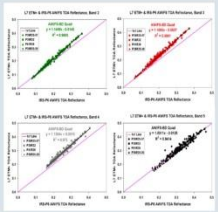

Comparison of TOA reflectance measurements from large ROIS common to the ETM+ and AWiFS sensors.

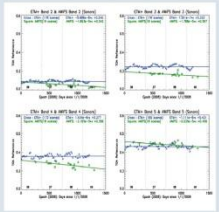

Long-term TOA Reflectance Trending over Sonoran site

Geometric Assessment

- Completed using the Image Assessment System (IAS) which was developed for Radiometric and Geometric Characterization and Calibration for the Landsat Program
- Image to Image (I2I) registration assessment tool
  - I2I is usually performed to compare the registration between two images
  - One image is selected as reference and another as the search image
  - Image chips are selected from reference image and are correlated with search image
  - The co-registration results provide an insight to the relative accuracy of the search image with respect to the reference image
  - When the correlated points are plotted in the image, it also helps to detect any systematic bias in the image
- Band to Band (B2B) registration assessment tool
  - B2B is performed to ensure that the proper band alignment parameters are provided
  - It is typically done by registering each band against every other band

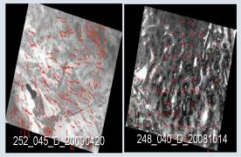

Vector residuals between AWiFS and GLS 2000 mosaic images over Sonoran and RVPN test site showing the direction and the distribution of errors (Note the vector scale: 1:500).

Mean, standard deviation, and RMSE for I2I results over Sonoran and RVP with respect to GLS2000 dataset.

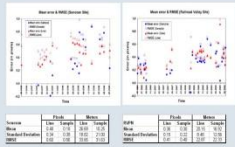

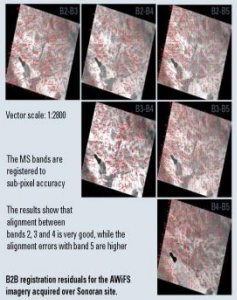

Vector scale: 1:2800

The MS bands are registered to sub-pixel accuracy

The results show that alignment between bands 2, 3 and 4 is very good, while the alignment errors with band 5 are higher

B2B registration residuals for the AWiFS imagery acquired over Sonoran site.

Summary

- Geometric Assessment
  - Image-to-Image (I2I) Assessment [registered to within one pixel]
  - Band to Band (B2B) Assessment [registered to within sub-pixel]
- AWiFS Dual Camera Radiometric Consistency Check [within 1% in most cases]
- Cross-calibration between ETM+ and AWiFS [B2=14.69%, B3=16.93%, B4=13.04%,B5=3.11%]
- Long-term TOA Reflectance Trending [shows degradation]

USGS
science for a changing world

Comparison of Landsat 5 TM and IRS-P6 AWiFS images for Landsat Data Continuity Studies

Xuexia Chen[1], James E. Vogelmann[2], Gyanesh Chander[3], Matthew Rollins[2], Lei Ji[1], Brian Tolk[3], Chengquan Huang[4]

1 ASRC Research and Technology Solution (ARTS), contractor to the U.S. Geological Survey (USGS) Earth Resources Observation and Science (EROS) Center, SD, USA. Work performed under USGS contract 08HQCN0007.
2 USGS EROS Center, SD, USA. 3 Stinger Ghaffarian Technologies (SGT), contractor to the USGS EROS Center, SD, USA. Work performed under USGS contract G10PC00044. 4 Department of Geography, University of Maryland, MD, USA.

Introduction

A gap in Landsat coverage during the next several years is a strong possibility because of the current and potential operating problems of the Landsat 5 and Landsat 7 sensors. We investigated the potential of Indian Remote Sensing Satellite P6 (IRS-P6) Advanced Wide Field Sensor (AWiFS) data as a substitute for Landsat data. The AWiFS sensor has 4 bands at 56 m resolution, which spectral detection ranges are very similar to Landsat bands 2-5.

Study area and data

Our study site was the common area of a Landsat scene and an AWiFS scene in the Los Angeles, California, area (fig. 1). This area has a considerable amount of urban, forest, agriculture, shrub, desert, and barren covers.

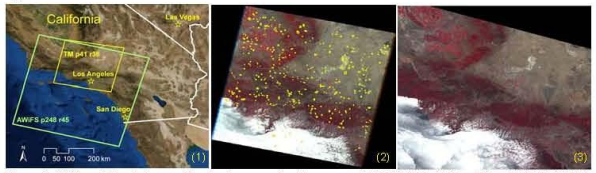

Figure 1. (1) Map of the study area. The two frames outline the scenes of L5 TM (Path 41 Row 36) and IRS-P6 AWiFS (Path 248 Row 45) images. (2) Landsat image with 500 manually sampled polygons. (3) AWiFS image subset.

Landsat 5 Thematic Mapper (TM) and IRS-P6 AWiFS images were obtained for this site (table 1). For the cross-sensor comparison, we used one Landsat scene and one AWiFS scene acquired nearly simultaneously on May 29, 2007.

Table 1. List of L5 TM and IRS-P6 AWiFS images acquired for the study site.

Sensor	Acquisition Date	Acquisition Time (Pacific Daylight Time)	Path/Row	Cloud Cover	Sun Azimuth Angle (degree)	Sun Elevation Angle (degree)
TM	2005/05/23	11:15:41 AM	P41R36	10%	112.6	65.9
TM	2006/05/26	11:20:35 AM	P41R36	20%	114.6	66.1
TM	2007/05/29	11:22:40 AM	P41R36	20%	118.1	66.7
AWiFS	2007/05/29	11:54:12 AM	P248 R45	15%	129.9	72.5
TM	2008/05/31	11:16:25 AM	P41R36	0%	115.0	65.8
TM	2009/06/19	11:16:44 AM	P41R36	11%	111.1	65.9

Methods

All data were processed to top-of-atmosphere (TOA) reflectance. Normalized Difference Vegetation Index (NDVI) was calculated for both 2007 images using the red and near-infrared TOA reflectance data (Rouse et al., 1974). Scene-dependent relative radiometric correction was developed by comparing 500 manually selected homogeneous polygons of two images (fig.1). In addition, to evaluate the scene-dependent correction results, the temporally invariant cluster (TIC) method (Chen et al. 2005) was used to investigate the NDVI relationships between the two images. The scene-independent correction functions from a previous study (Chander et al. 2009) were also used to compare with the scene-dependent method to determine image agreement. During the image agreement assessment, TM and AWiFS TOA reflectance images were resampled to 840 m resolution, which is the least common multiple of 56 m and 30 m resolutions. The image agreement assessment method (Ji and Gallo, 2006) was adopted to evaluate the agreement between TM and AWiFS images. Two images have perfect agreement if the Agreement Coefficient (AC) equals 1; they have poor agreement if the AC value is less than or equal to 0.

We resampled the relative radiometrically corrected 2007 AWiFS image to 30 m resolution using the bilinear method. By investigating the bands' correlation statistics of usable polygons in the 2007 Landsat TM image, we chose the resampled 30 m AWiFS band 2 to simulate TM band 1, and band 5 to simulate TM bands 6 and 7 because of their high correlations. Then, the 30 m Landsat-like AWiFS image was generated and used in the Landsat Time Series Stack (LTSS) from 2005 to 2009 for the Vegetation Change Tracker (VCT) model, which is a highly automated algorithm to detect forest disturbance (Huang et al., 2010).

Analysis and results

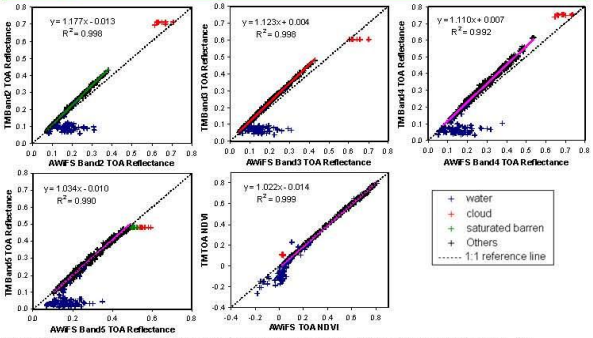

Figure 2. Comparison between AWiFS and TM images based on 500 polygons in homogeneous areas. The regression lines were generated by excluding the water, cloud, and saturated barren polygons.

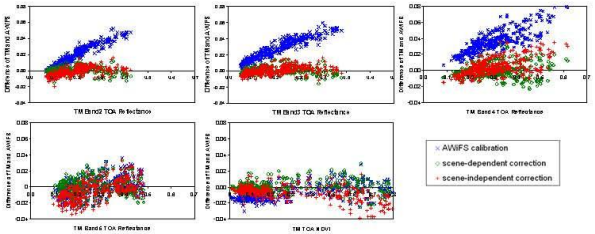

Figure 3. TOA reflectance comparison of usable polygons among original, scene-dependent, and scene-independent relative radiometrically corrected images.

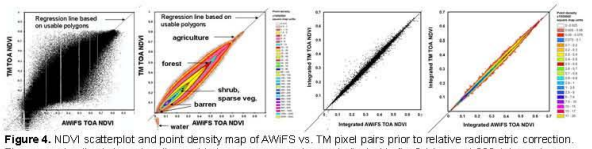

Figure 4. NDVI scatterplot and point density map of AWiFS vs. TM pixel pairs prior to relative radiometric correction. The regression line is based on the usable homogeneous polygons indicated in fig. 2 (slope = 1.022, intercept = –0.014). The TIC centers and dense ridges of barren, shrub, sparse vegetation, forest, and agriculture lie on the regression line. The integrated TM and AWiFS graphs are at 840 m resample resolution.

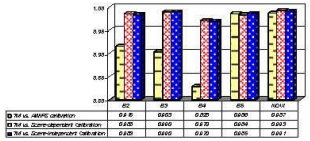

Figure 5. Image agreement assessment among resampled 840 m resolution TM, AWiFS, scene-dependent calibrated AWiFS, and scene-independent calibrated AWiFS images.

Subset of TM image in 2007 Bands 4, 3, and 2

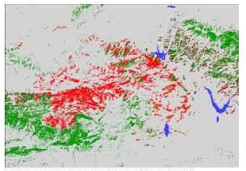

VCT outputs by LTSS from 2005-2009

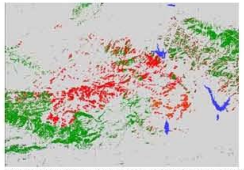

VCT outputs by LTSS with the substitute of 2007 AWiFS image (scene-dependent correction)

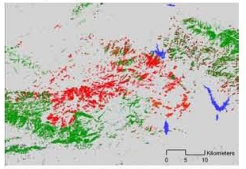

VCT outputs by LTSS with the substitute of 2007 AWiFS image (scene-independent correction).

Figure 6. Comparison of Vegetation Change Tracker (VCT) outputs using different data stacks. The area includes a fire scar area from a fire that burned in September 2006 (grey area in the false color composite).

Conclusions and future work

This poster indicates that we can effectively integrate AWiFS and Landsat data for long-term land cover characterization efforts. In general, AWiFS provides slightly lower TOA reflectance values than TM TOA reflectance for green, red, and NIR bands, especially for bright targets. These differences should be considered and corrected if the data are to be analyzed in conjunction with Landsat data. Landsat TM and AWiFS SWIR and NDVI data are very similar and can be used together without major modifications depending on the application. Both scene-dependent and scene-independent methods can be used to correct the systematic differences, but some minor unsystematic errors cannot be removed during the relative radiometric correction.

The scene-dependent correction by homogeneous polygons matches well with the TIC method by the density map of overlaid pixel values in TM and AWiFS images. These two methods can be used to provide accurate correction when a base image is available. The scene-independent method can be used to provide satisfactory relative radiometric correction when a base image is not available, or if results are needed reasonably quickly.

The application of AWiFS data for VCT analysis showed that AWiFS has the potential to substitute for Landsat data if appropriate Landsat data are not available. The data stacks that incorporated AWiFS data generated similar disturbance results to those generated using the LTSS. Future work is planned to adapt VCT for analysis using multisensor datasets.

Acknowledgement

Funding support for this study was provided by the U.S. Geological Survey and the LANDFIRE Operations and Maintenance project, which was sponsored by the Wildland Fire Leadership Council of the United States. Any use of trade, product, or firm names is for descriptive purpose only and does not imply endorsement by the U.S. government.

Reference

Chander, G., Xiong, X., Angal, A., Choi, T., & Malla, R. (2009). Cross-comparison of the IRS-P6 AWiFS sensor with the L5 TM, L7 ETM+, and Terra MODIS sensors. Proceeding of SPIE, 7474, 74740Z.

Chen, X., Vierling, L., & Deering, D. (2005). A simple and effective radiometric correction method to improve landscape change detection across sensors and across time. Remote Sensing of Environment, 98, 63-79.

Ji, L., & Gallo, K. (2006). An agreement coefficient for Image comparison. Photogrammetric Engineering and Remote Sensing, 72, p823-833.

Huang, C., Goward, S., Masek, J.G., Thomas, N., Zhu, Z., & Vogelmann, J.E. (2010). An automated approach for reconstructing recent forest disturbance history using dense Landsat time series stacks. Remote Sensing of Environment, 114, 183-198.

Rouse, J. W., Haas, R. H., Schell, J. A., & Deering, D. W. (1974). Monitoring vegetation systems in the Great Plains with ERTS. Greenbelt: NASA SP-351.

Remote Sensing Technologies

understanding the technologies needed to sense our world

Google™ Custom Search Search

Joint Agency Commercial Imagery Evaluation (JACIE)

The growing number of commercial sources for remotely sensed data offers users more choices than ever before. The key to using data from these new sources is understanding their characteristics and capabilities, and the quality of the data they produce.

The Joint Agency Commercial Imagery Evaluation (JACIE) program was formed to leverage Federal agencies' resources for the characterization of commercial remote sensing data and to share those results across the Federal Government and beyond. Consisting of representatives from the U.S. Geological Survey (USGS), the National Aeronautics and Space Administration (NASA), the National Geospatial-Intelligence Agency (NGA), and the U.S. Department of Agriculture (USDA), the JACIE team performs product analysis of commercial and other remote sensing data and information products, providing earth scientists and other users with awareness and independent verification of commercial imagery data quality.

The JACIE team provides independent characterizations of delivered image and image-derived end products. Each team member agency brings their resources and strengths to this task, providing Federal users in-depth assessments of commercial imagery quality. JACIE team efforts have been instrumental in several improvements to commercial image product quality and have enhanced working relationships between government and the commercial remote sensing industry.

Results of JACIE evaluations are presented at the annual JACIE Civil Commercial Imagery Evaluation Workshop.

JACIE 2012

Proceedings From Previous JACIE Workshops

- November 8-10, 2004
- March 14-16, 2006
- March 20-22, 2007
- March 25-27, 2008
- March 31 – April 2, 2009
- March 16 – 18, 2010
- March 29 – 31, 2011

JACIE 2012
April 17 – 19, 2012
Fairfax, Virginia

JACIE 2013
April 16-18, 2013
St. Louis, MO

RECENT NEWS

- USGS National Test Ranges
- JACIE 2012
- RST Project supports global quality standards for earth observation data
- IEEE TGRS Special Issue on "Inter-Calibration of Satellite Instruments"
- USGS Announces "No USGS Digital Camera Certification Requirement"
- USGS Will Continue to Provide Film Camera Calibration Services
- USGS RST ASPRS 2010 Paper Featured by GISCafe
- Joint Agency Commercial Imagery Evaluation (JACIE) Workshop Agenda
- Successful GSICS Working Group Meeting in Daejeon, South Korea
- 15th Annual NASA LCLUC Science Team Meeting

BROWSE ARCHIVES

January 2012

BROWSE CATEGORIES

- About Us
- Aerial
- Highlights
- JACIE
- News
- Reports
- Satellite

Special issue of the CJRS: "Terrestrial Reference Standard Test Sites for Post-Launch Calibration"

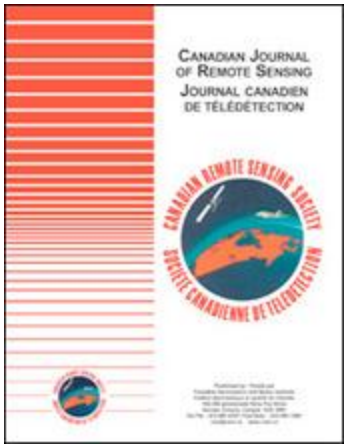

The paper submission deadline for this special issue was February 18, 2010. It was published in Oct. 2010

For this edition, the domain of interest is limited to IVOS.

This special journal issue focussed on how test sites provide important and convenient post-launch means of obtaining information to verify the performance of sensors.

Announcement / Annonce

Call for papers
Special issue of the *Canadian Journal of Remote Sensing*

Terrestrial reference standard test sites for post-launch calibration

Guest Editors

Gyanesh Chander
SGT, Contractor to the
U.S. Geological Survey (USGS), USA
E-mail: gchander@usgs.gov

Philippe M. Teillet
University of Lethbridge, Alberta, Canada
E-mail: p.teillet@uleth.ca

In an era when the number of Earth-observing satellites is rapidly growing, and measurements from these sensors are used to answer increasingly urgent global issues, often through synergistic and operational combinations of data from multiple sources, it is imperative that scientists and decision-makers be able to rely on the accuracy of Earth observation data products. The characterization and calibration of these sensors, particularly their relative biases, are vital to achieving the development of the integrated Global Earth Observation System of Systems (GEOSS) for coordinated and sustained observations of the Earth. This can only be reliably achieved in the post-launch environment through the careful use of observations by multiple sensor systems over common and well-characterized terrestrial targets.

Earth surfaces with suitable characteristics have long served as benchmark or reference standard test sites to verify the post-launch radiometric calibration performance of satellite sensors. Reference standard test sites are a key operational component of the newly established Quality Assurance Framework for Earth Observation (QA4EO). At present, test sites in their broadest sense are the only practical means of deriving knowledge on biases between sensors in all technical domains and provide a convenient means of obtaining information to verify sensor performance. Accordingly, this special journal issue will focus on how reference standard test sites provide important and convenient post-launch means of obtaining information to verify the performance of sensors. For this edition, the domain of interest is limited to infrared, visible, and optical sensors.

The Guest Editors invite submissions that explore topics including, but not limited to, vicarious calibration, radiometric and geometric stability monitoring, land and sea surface temperature, modulation transfer function (MTF), geolocation, signal-to-noise ratio (SNR), band-to-band, stray light, spectral, uniformity, and temporal effects. If you intend to submit a

Appel d'articles
Numéro spécial du *Journal canadien de télédétection*

Sites témoins terrestres pour l'étalonnage post-lancement

Rédacteurs invités

Gyanesh Chander
SGT, Consultant auprès
du U.S. Geological Survey (USGS), É.-U.
Courriel : gchander@usgs.gov

Philippe M. Teillet
University of Lethbridge, Alberta, Canada
Courriel : p.teillet@uleth.ca

À une époque où le nombre de satellites d'observation de la Terre augmente sans cesse et alors que les mesures de ces capteurs sont utilisées pour répondre à des problématiques de plus en plus urgentes à l'échelle du globe, la plupart du temps en ayant recours à des combinaisons synergiques et opérationnelles de données de sources multiples, il est impératif que les scientifiques et les décideurs soient capables de compter sur la précision des produits de données d'observation de la Terre. La caractérisation et l'étalonnage de ces capteurs, particulièrement de leurs biais relatifs, sont des éléments essentiels pour assurer le développement du système intégré GEOSS (Système des systèmes mondiaux d'observation de la Terre) pour des observations coordonnées et durables de la Terre. Ceci ne peut être accompli de façon fiable, dans un environnement post-lancement, que par l'utilisation prudente d'observations réalisées à l'aide de systèmes de capteurs multiples au-dessus de cibles terrestres communes et bien caractérisées.

Les surfaces terrestres présentant des caractéristiques adéquates ont souvent servi comme repères ou sites témoins pour vérifier la performance de l'étalonnage radiométrique post-lancement des capteurs satellitaires. Les sites témoins sont une composante opérationnelle importante de l'initiative QA4EO (« Quality Assurance Framework for Earth Observation ») récemment mise en place. À l'heure actuelle, les sites tests au sens le plus large du terme constituent en pratique le seul moyen d'obtenir de l'information sur les biais entre les capteurs dans tous les domaines techniques et ces derniers constituent un moyen pratique d'acquisition d'information permettant de vérifier la performance des capteurs. Ainsi, l'objet de ce numéro spécial de la revue sera de montrer comment les sites témoins peuvent constituer une source importante et pratique pour l'obtention d'informations dans le contexte de la vérification post-lancement de la performance des capteurs. Pour cette édition, le champ

Special issue of the IEEE TGRS: "Inter-Calibration of Satellite Instruments"

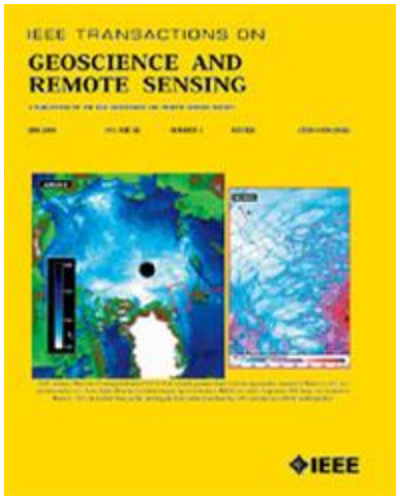

The paper submission deadline for this special issue was January 31, 2012, with a target publishing date of early 2013.

This special journal issue will focus on how inter-calibration and comparison between sensors can provide an effective and convenient means of verifying post-launch sensor performance and correcting the differences.

CALL FOR PAPERS

IEEE Transactions on Geoscience and Remote Sensing

Special Issue on "Inter-Calibration of Satellite Instruments"

The ability to detect and quantify changes in the Earth's environment using remote sensing is dependent upon sensors providing accurate and consistent measurements over time. A critical step in providing these measurements is establishing confidence and consistency between data from different sensors and putting them onto a common radiometric scale. However, ensuring that this process can be relied upon long term and that there is physical meaning to the information requires traceability to internationally agreed, stable, reference standards ideally tied to the international system of units (SI). This requires robust on-going calibration, validation, stability monitoring, and quality assurance, all of which need to be underpinned and evidenced by comparisons involving a reference standard or sensor and a methodology with defined uncertainty (in an absolute or temporal sense). This process can be used to provide calibrations to other sensors (i.e. Inter-calibration).

Inter-calibration and comparisons between sensors have become a central pillar in calibration and validation strategies of national and international organizations. The Global Space-based Inter-Calibration System (GSICS) is an international collaborative effort initiated by World Meteorological Organization (WMO) and the Coordination Group for Meteorological Satellites (CGMS) to monitor and harmonize data quality from operational weather and environmental satellites. The Infrared Visible Optical Sensors (IVOS) sub-group of the Committee on Earth Observation Satellites (CEOS) Working Group on Calibration and Validation (WGCV) extends this vision to include all Earth observation sensors and satellite operating agencies. Inter-calibration techniques provide a practical means of correcting biases between sensors and bridging any potential data gaps between non-contiguous sensors in a critical time-series and the inter-calibration reference serves as a transfer standard. It is expected that promotion of the use of robust inter-calibration techniques will lead to improved consistency between satellite instruments, reduce overall costs, and facilitate accurate monitoring of planetary changes.

List of topics

Contributions for this special issue are welcome from the research community. This special journal issue will focus on how inter-calibration and comparison between sensors can provide an effective and convenient means of verifying post-launch sensor performance and correcting the differences. The guest editors invite submissions that explore topics including, but not limited to, pseudo-invariant calibration sites, instrumented sites, simultaneous nadir observations and other ray-matching comparisons, lunar and stellar observations, deep convective clouds, liquid water clouds, Rayleigh scattering and Sun glint. The inter-calibration results should focus on rigorous quantification of bias and associated sources of uncertainty from different sensors, crucial for long-term studies of the Earth. The goal of this special journal issue is to capture the state-of-the-art methodologies and results from inter-calibration of satellite instruments, including full end-to-end uncertainty analysis. Accordingly, it will become a reference anthology for the remote sensing community.

Paper submission deadline: 31 January 2012

Submission guidelines

Normal page charges, peer-review, and editorial process will apply. Prospective authors should follow the regular guidelines of TGRS, and should submit their manuscripts electronically to *http://mc.manuscriptcentral.com/tgrs*. Please indicate during your submission that the paper is intended for this Special Issue. Inquiries with respect to the special issue should be directed to the Guest Editors.

Guest Editors

Gyanesh Chander, Ph.D.
Lead Systems Engineer
SGT/USGS EROS
47914 252nd St.
Sioux Falls, SD, 57198 USA
Phone: 605-594-2554
Email: gchander@usgs.gov

Tim Hewison, Ph.D.
Meteorological Scientist
EUMETSAT
Eumetsat-Allee 1
64295 Darmstadt, Germany
Phone: +49 6151 807 364
Email: tim.hewison@eumetsat.int

Nigel Fox, Ph.D.
Head of Earth Observation
National Physical Laboratory
Hampton Rd, Teddington
Middx, TW11 0LW, UK
Phone: +44 208 943 6825
Email: nigel.fox@npl.co.uk

Xiangqian (Fred) Wu, Ph.D.
Physical Scientist
STAR/NESDIS/NOAA
E/RA2, 7214, 5200 Auth Rd.
Camp Springs, MD 20746 USA
Phone: 301-763-8136 ext. 138
Email: Xiangqian.Wu@noaa.gov

Xiaoxiong (Jack) Xiong, Ph.D.
Optical Physicist
NASA GSFC
Code 614.4,
Greenbelt, MD, 20771, USA
Phone: 301-614-5957
Email: Xiaoxiong.Xiong-1@nasa.gov

William J. Blackwell, Sc.D.
Associate Editor, IEEE TGRS
MIT Lincoln Laboratory
244 Wood St., S4-225
Lexington, MA 02420, USA
Phone: 781-981-7973
Email: WJB@LL.MIT.EDU

Summary & USGS Key Involvement

- **USGS has extensive internal capabilities and leads a number of national and international calibration partnership and activities**
- **Lead a number of GEOSS Quality Assurance Strategy sub-tasks**
- **Landsat Cross-calibration Activities**
  - On-going Cross-calibration Activities:
    - IRS-P6 AWiFS/LISS-III, CBERS-2/B CCD, ALOS AVNIR-2, UK DMC-1/2, RapidEye Constellation, SPOT, Worldview, MODIS, ALI, THEOS MS sensors
  - Planned Cross-calibration Activities
    - Landsat TM/ETM+ with: LDCM, Sentinel, ENVISAT MERIS, AVHRR MetOP, Cartosat-2, ResourceSat-2, CBERS-3, etc.
- **Landsat archive and open data policy has enabled growth and innovation in use and applications of land remote sensing data**
- **Goal to establish an operational Landsat program**